Volume transport of the Antarctic Circumpolar Current: Production and validation of a 20 year long time series obtained from in situ and satellite observations

Zoé Koenig, Christine Provost, Ramiro Ferrari, Nathalie Sennéchael, Marie-Hélène Rio

AGU PUBLICATIONS

JGR

Journal of Geophysical Research: Oceans

RESEARCH ARTICLE

10.1002/2014JC009966

Key Points:
- ACC transport time series
- Combination of in situ and satellite data
- Development of a look-up table

Correspondence to:
Z. Koenig,
zklod@locean-ipsl.upmc.fr

Citation:
Koenig, Z., C. Provost, R. Ferrari, N. Sennéchael, and M.-H. Rio (2014), Volume transport of the Antarctic Circumpolar Current: Production and validation of a 20 year long time series obtained from in situ and satellite observations, *J. Geophys. Res. Oceans*, *119*, 5407–5433, doi:10.1002/2014JC009966.

Received 12 MAR 2014
Accepted 9 JUL 2014
Accepted article online 14 JUL 2014
Published online 25 AUG 2014

Volume transport of the Antarctic Circumpolar Current: Production and validation of a 20 year long time series obtained from in situ and satellite observations

Zoé Koenig[1], Christine Provost[1], Ramiro Ferrari[1], Nathalie Sennéchael[1], and Marie-Hélène Rio[2]

[1]Laboratoire LOCEAN-IPSL, Sorbonne Universités (UPMC, Univ. Paris 6)-CNRS-IRD-MNHN, Paris, France, [2]CLS Argos, Ramonville, Saint-Agne, France

Abstract A 20 year long volume transport time series of the Antarctic Circumpolar Current across the Drake Passage is estimated from the combination of information from in situ current meter data (2006–2009) and satellite altimetry data (1992–2012). A new method for transport estimates had to be designed. It accounts for the dependence of the vertical velocity structure on surface velocity and latitude. Yet unpublished velocity profile time series from Acoustic Doppler Current Profilers are used to provide accurate vertical structure estimates in the upper 350 m. The mean cross-track surface geostrophic velocities are estimated using an iterative error/correction scheme to the mean velocities deduced from two recent mean dynamic topographies. The internal consistency and the robustness of the method are carefully assessed. Comparisons with independent data demonstrate the accuracy of the method. The full-depth volume transport has a mean of 141 Sv (standard error of the mean 2.7 Sv), a standard deviation (std) of 13 Sv, and a range of 110 Sv. Yearly means vary from 133.6 Sv in 2011 to 150 Sv in 1993 and standard deviations from 8.8 Sv in 2009 to 17.9 Sv in 1995. The canonical ISOS values (mean 133.8 Sv, std 11.2 Sv) obtained from a year-long record in 1979 are very similar to those found here for year 2011 (133.6 Sv and 12 Sv). Full-depth transports and transports over 3000 m barely differ as in that particular region of Drake Passage the deep recirculations in two semiclosed basins have a close to zero net transport.

1. Introduction

The Southern Ocean receives more than 70% of the work exerted by the wind on the global ocean [*Wunsch*, 1998] and hosts the largest ocean current, the Antarctic Circumpolar Current (ACC). The ACC is the only current without latitudinal barriers, connecting the deep waters of the three major oceans. The ACC separates the warm subtropical waters from the cold Antarctic waters, thermally isolating the Antarctic Continent. Nevertheless, the ACC plays a major role in the thermohaline circulation of the world's oceans [*Morrison and Hogg*, 2013; *Toggweiler and Samuels*, 1995].

An increase in the circumpolar westerly winds has been observed since the 1970s [*Thompson and Solomon*, 2002], corresponding to a larger Southern Annular Mode (SAM) index (http://www.nerc-bas.ac.uk/icd/gjma/sam.html). Low-resolution models predict that the wind strengthening could lead to an increased ACC transport [*Hall and Visbeck*, 2002; *Fyfe and Saenko*, 2007]. However, it has been suggested that the strengthening of the winds generates an increase in the ACC eddy activity, so that the ACC reaches a saturation eddy state [*Hallberg and Gnanadesikan*, 2006; *Meredith and Hogg*, 2006; *Yang et al*., 2007]. Indeed, high-resolution numerical studies show little dependence of the ACC volume transport to zonal winds [*Morrison and Hogg*, 2013; *Munday et al*., 2013]. Nonetheless, the lack of observations does not allow to document a trend of eddy activity in the Southern Ocean since the 1970s.

In this context, long-term time series of the ACC volume transport are needed. Yet, because of the inhospitality of the Southern Ocean, data are sparse and monitoring the ACC is a difficult task. Historically, the ACC is mainly monitored in the Drake Passage, the most convenient location for studying the ACC because of its narrowness (Figure 1). One of the first program developed in the Southern Ocean was the ISOS program (International Southern Ocean Study) from 1974 to 1981 which provided mooring data during 1 year in the Drake Passage, and several hydrographic surveys [*Nowlin et al*., 1977; *Bryden*, 1979; *Whitworth*, 1983]. These data led to the first description of vertical and horizontal structures of the ACC. Three fronts were identified

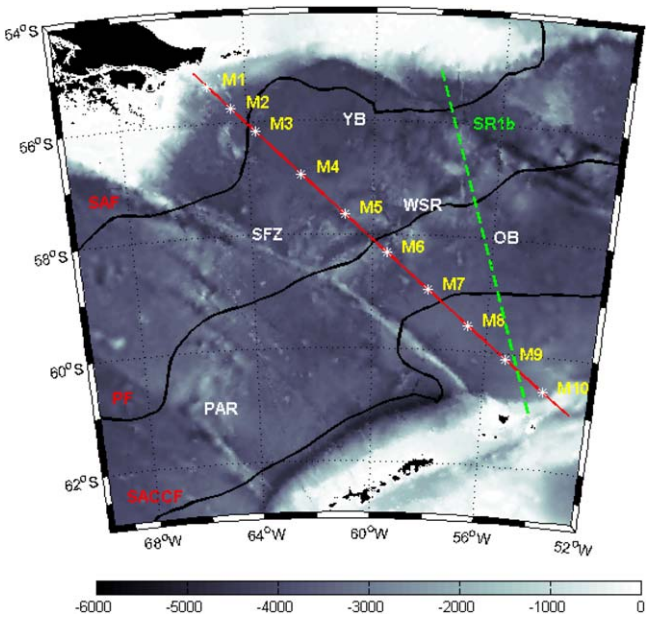

Figure 1. Bathymetry in the Drake Passage in meters. In red, Jason satellite ground track 104 where an asterisk indicates a mooring location (M1 through M10). In green, the SR1b annually repeated hydrography line [*Cunningham et al.*, 2003]. OB, Ona Basin; YB, Yaghan Basin; SFZ, Shackleton Fracture Zone; WSR, West Scotia Ridge; PAR, Phoenix Atlantic Ridge. The black lines represent the mean location of the fronts [*Orsi et al.*, 1995]. SAF, Subantarctic Front; PF, Polar Front; SACCF, Southern ACC Front.

from north to south [*Nowlin et al.*, 1977]: the Subantarctic Front (SAF), the Polar Front (PF), and the Southern ACC Front (SACCF) (Figure 1). The ISOS program provided the first estimation of the mean and standard deviation of the total ACC volume transport at Drake Passage: 134 Sv with a standard deviation of 11 Sv for a year-long record [*Whitworth et al.*, 1982; *Whitworth*, 1983; *Whitworth and Peterson*, 1985]. The range of uncertainty on the mean was later established to lie between 15 and 27 Sv [*Cunningham et al.*, 2003].

Most subsequent estimations of the volume transport concerned the baroclinic component. From the annually repeated hydrographic transect SR1b in the western Drake Passage (WOCE program) between 1993 and 2000 (Figure 1), *Cunningham et al.* [2003] estimated the baroclinic transport referenced to the bottom to be 136.7 Sv with a standard deviation of 7.8 Sv. However, evaluation of the total volume transport requires velocity information. The few studies estimating the total volume transport have provided similar values to that of the ISOS program, mostly between 130 Sv and 150 Sv [*Cunningham et al.*, 2003; *Renault et al.*, 2011], and sparse observations do not indicate any long-term trend [*Meredith et al.*, 2011].

Chouaib et al. [2006] used the satellite altimetric time series to estimate the surface volume transport of the ACC in the Drake Passage. They did not detect any trend in the surface transport but remarked an anticorrelation between the SAF and PF volume transport. They obtained the canonical value of 134 Sv for the mean total volume transport when the surface transport is extrapolated to the bottom using an e-folding depth of 750 m.

The main goal of the DRAKE project is to take advantage of the 20 year long homogeneous altimetric time series initiated in 1992 to estimate a volume transport time series of the ACC in Drake Passage. Hydrographic data and current meter time series were collected during 3 years (2006–2009) in the water column below the ground track 104 of Jason altimetry satellite (Figure 1). The in situ data are located downstream of the Shackleton Fracture Zone (SFZ) in the Yaghan Basin north of the West Scotia Ridge (WSR) and in the Ona Basin south of the WSR (Figure 1).

The DRAKE in situ data were used to evaluate the altimetric products. Both hydrographic data and current meter data showed that altimetric data, and in particular multisatellite gridded products provided accurate information on sea surface height and surface velocity variations [*Barré et al.*, 2011; *Ferrari et al.*, 2012, 2013]. The satisfactory comparison with altimetry derived surface velocities and a high vertical coherence of the horizontal velocity revealed by the current meter data have been shown to be encouraging in terms of computation of the full-depth volume transport.

This paper aims to combine in situ and satellite data to produce a 20 year long time series of volume transport and estimate their basic statistics and spatial distribution relative to current fronts as well as the baroclinic/barotropic partition of the ACC transport in Drake Passage. Previously, *Spadone and Provost* [2009] and *Vivier and Provost* [1999] used combined information from current meters and altimetric data to

Table 1. Nominal Position, Water Depth, and Number of Days of Data Recoveries (Third Column: During 2006–2008, Fourth Column During 2008–2009) of the Current Meters Along the Jason Satellite Ground Track 104 From North to South[a]

Mooring	Depth (m)	Number of Days (2006–2008)	Number of Days (2008–2009)
M1	60 (ADCP)	789	345
55°20′51″S	500	789	345
65° 11′15″W	1000	434	345
M2	450		343
55°43′13″S	1000		343
64° 24′10″W	2000		343
M3	380 (ADCP)	812	344
56°07′92″S	500		344
63° 42′66″W	1000	812	344
	2000	812	344
	3000		344
M4	500	809	334
56°56′54″S	1000	809	334
62° 19′61″W	2500	809	334
M5	500	778	345
57°37′63″S	1000	778	345
60°55′26″W	2500	778	345
M6	235	805	
58°19′47″S	820	805	
59°31′12″W	2410	805	
M7	460	690	
58°57′29″S	980	690	
58°06′04″W	2515	803	
M9	1045	800	
60°06′06″S	2510	800	
55°15′49″W			
M10	460	394	
60°37′12″S	1000	394	
53°50′59″W	2560	394	

[a]Details of the ADCP data are given in Table 2.

compute a time series of volume transport of the Malvinas Current. However, their method relies on a section of mean velocities estimated from the current meter data. This section of mean velocity cannot been obtained in Drake Passage from only nine moorings where flow variability is energetic and of small spatial scales. Hence, a new method is deemed necessary to estimate the volume transport in Drake Passage. The objective of this study is to describe the applied methodology, show its robustness, and present the times series and their basic statistics. Examining the dynamical drivers of the observed variability is beyond the scope of this paper and is the object of a companion paper (Z. Koenig et al., manuscript in preparation, 2014).

The paper is organized as follows: section 2 presents the data and the new method used to estimate volume transport time series. The yet unpublished 3 year long velocity profile time series in the upper 350 m collected from Acoustic Doppler Current Profilers (ADCP) are presented in section 3. These data provide precise information on the vertical structure of the upper 350 m. In section 4, velocity profiles at each mooring are binned based on the surface velocity to construct a "look-up" table of velocity profiles. A mean surface velocity is adjusted iteratively to fit the in situ data. The method is then validated against independent data. In section 5, a time series of volume transport is constructed using the 20 years of altimetric data and analyzed for its statistics. Section 6 discusses the robustness of the method and its limitations. Conclusions are given in section 7.

2. Data and Method

2.1. Data

2.1.1. Mooring Data

The current meter array made up of nine moorings (M1 through M10, M8 being lost) was located under the Jason altimeter track 104, parallel to and downstream of the SFZ (Figure 1). These moorings gathered 3 years (2006–2009) of current velocity measurements in the Yaghan Basin [*Ferrari et al*., 2012] and 2 years (2006–2008) in the Ona Basin [*Ferrari et al*., 2013]. An Acoustic Doppler Current Profiler (ADCP) was settled in the uppermost subsurface buoy at M1 and M3 (Tables 1 and 2). In their analysis, *Ferrari et al*. [2012] only used one depth level of ADCP data. The whole ADCP data set which provides information on the upper 350 m of the water column is presented and analyzed in section 3.

An independent current meter is used for comparison: the bottom (4100 m depth) cDrake current meter in Drake Passage close to M4 [*Chereskin et al*., 2009; *Firing et al*., 2014].

2.1.2. LADCP Data

Lowered Acoustic Doppler Current Profilers (LADCP) sections were performed along track 104 during mooring recoveries/deployments. In particular, two high-resolution LADCP sections performed within 3 weeks in

Table 2. ADCP at Moorings (M1 or M3), Dates, Vertical Resolution, and Range (Minimum Depth and Maximum Depth)[a]

Mooring	Beginning	End	Step (m)	Minimum Depth (m)	Maximum Depth (m)
M1 06–08	17 Jan 2006	11 Apr 2008	5	15	60
M3 06–08	19 Jan 2006	9 Apr 2008	10	60	350
M1 08–09	13 Apr 2008	24 Mar 2009	15	60	435
M3 08–09	11 Apr 2008	26 Mar 2009	15	60	360

[a]In 2006–2008, we used an ADCP 300kHz WH5307 at M1 and an ADCP Narrow Band 514 at M3. In 2008–2009, we used an ADCP 75kHz WHLR3427 at M1 and WHLR1066 at M3.

2006, showed noticeable differences in velocity spatial distribution while the total transport barely changed [*Renault et al*., 2011]. These data are used as independent data to validate the method (section 4.3).

2.1.3. Satellite Data

Altimetric satellite data extend from the 14 October 1992 to the 7 August 2013. We used delayed-time gridded maps of sea level anomaly (MSLA) with a spatial resolution of $1/3^\circ \times 1/3^\circ$ on a Mercator grid at 7 day intervals. The products result from the merging of observations from several satellites. The number of available satellite varies from two from 1992 to 1999 to three or four from 2000 to 2012. The data come from the archiving, validation, and interpretation of satellite oceanographic data (AVISO) database (Collect-Localisation-Satellites, CLS Space Oceanography): www.aviso.oceanobs.com. The 7 day gridded products are preferred to the near 10 day repeat cycle along track product [*Barré et al*., 2011; *Ferrari et al*., 2012]. Gridded data are interpolated at the exact positions of the moorings and all along track 104 in the Drake Passage. Surface geostrophic velocities are calculated using the Mapped Absolute Dynamic Topography (MADT) which is the sum of the Sea Level Anomaly (SLA) and the Mean Dynamic Topography (MDT).

2.1.4. Mean Dynamic Topography (MDT)

Two MDTs are used here: the CNES-CLS09 MDT [*Rio et al*., 2011] and the recent CNES-CLS13 MDT [*Rio et al*., 2013]. The two MDTs were computed by combining altimeter, gravimeter, and in situ data using a three-step methodology described in *Rio et al*. [2011].

To begin with, a large-scale first guess is calculated from smoothing the direct differences between an altimeter Mean Sea Surface (MSS, the mean sea level above a reference ellipsoid) and a model of the geoid height above the same reference ellipsoid. Then, synthetic estimates of the mean dynamic topography and the mean geostrophic currents are obtained by removing the altimeter variability from instantaneous in situ measurements of the ocean state (dynamic heights calculated from temperature and salinity profiles, surface currents from drifting buoys). In the third step, these synthetic estimates are used to improve the large-scale first guess through a multivariate objective analysis.

For the CNES-CLS13 MDT, a number of improvements have been made possible by the use of updated and extended datasets and refined processing. In particular, the large-scale first guess was obtained by combining a GOCE geoid model from the fourth official ESA release [*Bruinsma et al*., 2004] and the CNES-CLS11 altimeter MSS [*Schaeffer et al*., 2012], instead of a GRACE geoid model and the CLS01 MSS for the CNES-CLS09 MDT computation. Next, the in situ data used to compute the synthetic mean observations consisted in hydrological profiles measured by ARGO floats and CTD/XBT casts as well as SVP-type drifting buoy data for the period 1993–2012, instead of 1993–2008 for the previous solution. The current velocities derived from the drift of Argo floats at the surface during data transmission have been included for the computation of this new solution. The in situ data were carefully processed in order to match the altimeter data physical content. Specifically, the surface velocities derived from the drifting buoy and Argo float trajectories were corrected from the Ekman current contribution and the direct wind slippage. The final solution was shown to compare better to independent in situ observations than the previous CNES-CLS09 MDT.

In the center of Drake Passage, the main differences between the two MDTs concern the recirculation cells: the CNES-CLS13 MDT captures the recirculation cells in the two basins, while the CNES-CLS09 MDT does not present any westward current in the Yaghan and Ona Basin (Figures 2a and 2b). The intensification of the two cyclonic cells is evidenced in the difference between the two MDT's (Figure 2c). The cross-track surface geostrophic velocities derived from the two MDTs have a mean difference of 0.2 cm/s (Figure 2d). Along

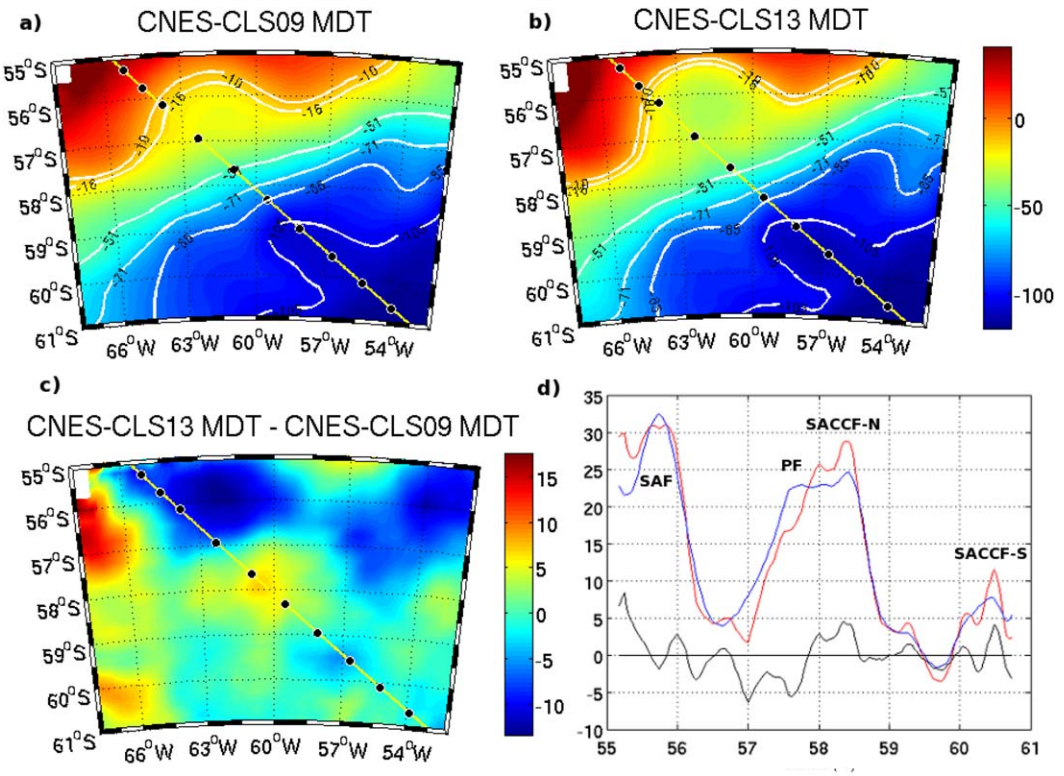

Figure 2. Maps of mean absolute dynamic topographies (color scale in cm). (a) CNES-CLS09 MDT. (b) CNES-CLS13 MDT. (c) Difference between the CNES-CLS13 MDT and the CNES-CLS09 MDT. In white, the position of the front branches, along isolines (determined by *Barré et al.* [2011]). From North to South, two branches of SAF, three branches of PF, and SACCF-N. The SACCF-S is not presented. In yellow, track 104 with the locations of the moorings (black dots). (d) Mean cross-track surface geostrophic velocities (blue and red) deduced from the two MDTs (in red for the CNES-CLS13 and in blue for the CNES-CLS09) and in black their difference. *X* axis is latitude along track 104 (°S), *y* axis is velocity in cm/s.

track 104, the PF is slightly more to the south, closer to the SACCF-N in the new MDT, the SAF, and SACCF-S positions are unchanged (Figure 2d).

2.2. Method

The volume transport through track 104 is estimated using both in situ and satellite data. Previously, in *Spadone and Provost* [2009], the across-track velocity $V(x, z, t)$ at track point x, depth z, and time t was estimated as:

$$V(x,z,t)=V_m(x,z)+A(x,z)V'(x,0,t) \quad (1)$$

where V_m is the perpendicular mean velocity through the section, $A(x, z)$ a function which characterizes the vertical structure of the current, and $V'(x,0,t)$ the surface geostrophic velocity anomaly obtained from satellite data. The relation (1) supposes a reliable and constant transfer function $A(x, z)$ with time and a good estimate of the mean velocity $V_m(x, z)$. This method, called classical method hereafter, was successfully applied to the Malvinas Current where the current is broad and steered by a steep topography [*Spadone and Provost*, 2009].

In Drake Passage, because of the important variability in space and time of the narrow fronts, the weak flow between the latter and the high quantity of eddies, a realistic mean velocity cannot be estimated a priori from only nine moorings.

Therefore, we use the following method with the cross-track velocity estimated as:

$$V(x,z,t)=B(x,z,V(x,0,t)) \quad \text{with} \quad V(x,0,t)=V_s(x,0)+V'(x,0,t) \quad (2)$$

where B is a function (named as look-up table B, see section 4.1.3) characterizing the velocity vertical structure which depends on the latitude x, the depth z, and the surface geostrophic velocities $V(x, 0, t)$. The

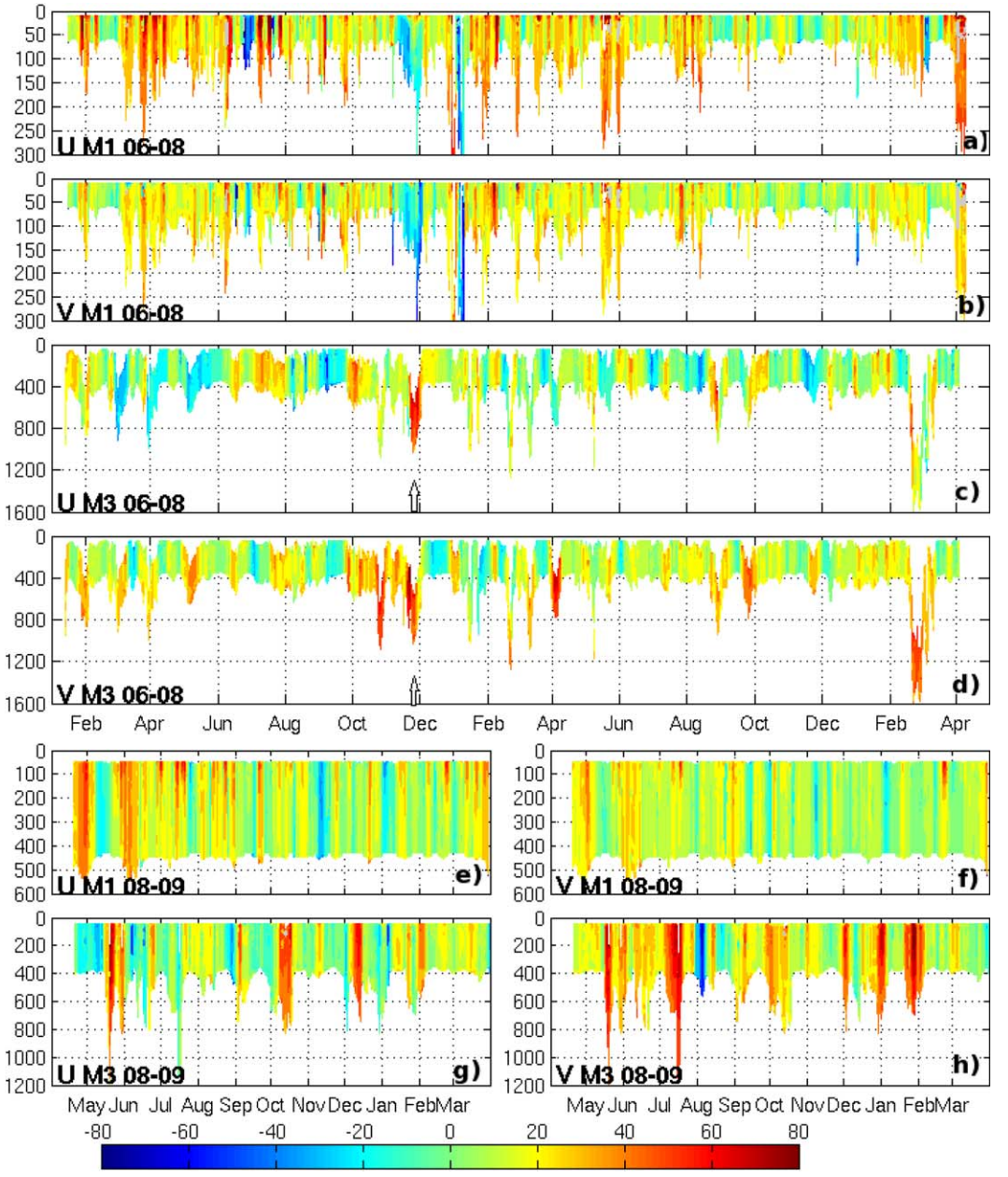

Figure 3. ADCP data at moorings M1 and M3. *X* axis is latitude along track 104, *y* axis is depth in meters. Velocities (colorbar) are in cm/s. Note that the vertical scale is not the same for all the plots. (a) Zonal velocity at M1 6 January to 8 April. (b) Meridional velocity at M1 6 January to 8 April. (c) Zonal velocity at M3 6 January to 8 April. (d) Meridional velocity at M3 6 January to 8April. (e) Zonal velocity at M1 8 April to 9 March. (f) Meridional velocity at M1 8 April to 9 March. (g) Zonal velocity at M3 8 April to 9 March. (h) Meridional velocity at M3 8 April to 9 March. The arrows represent events the paper talked about.

surface geostrophic velocity $V(x, 0, t)$ is the sum of $V'(x, 0, t)$ the surface geostrophic velocity anomaly deduced from the sea level anomaly obtained from satellite altimetry and a mean surface geostrophic velocity $V_s(x, 0)$ that can come from a MDT (e.g., CNES-CLS09 MDT or CNES-CLS13 MDT). The volume transport corresponds to the integral of these velocities $V(x, z, t)$ along track 104.

The method requires a good knowledge of the vertical velocity structure (section 4.1) and of the absolute surface geostrophic velocity (section 4.2). The vertical velocity structure estimates are obtained as a function of mooring (latitude), depth, and surface velocities at each mooring along track 104 using the 3 year-long velocity time series from the DRAKE project (section 4.1). We first examine the velocities in the upper 350 m using the ADCP data time series.

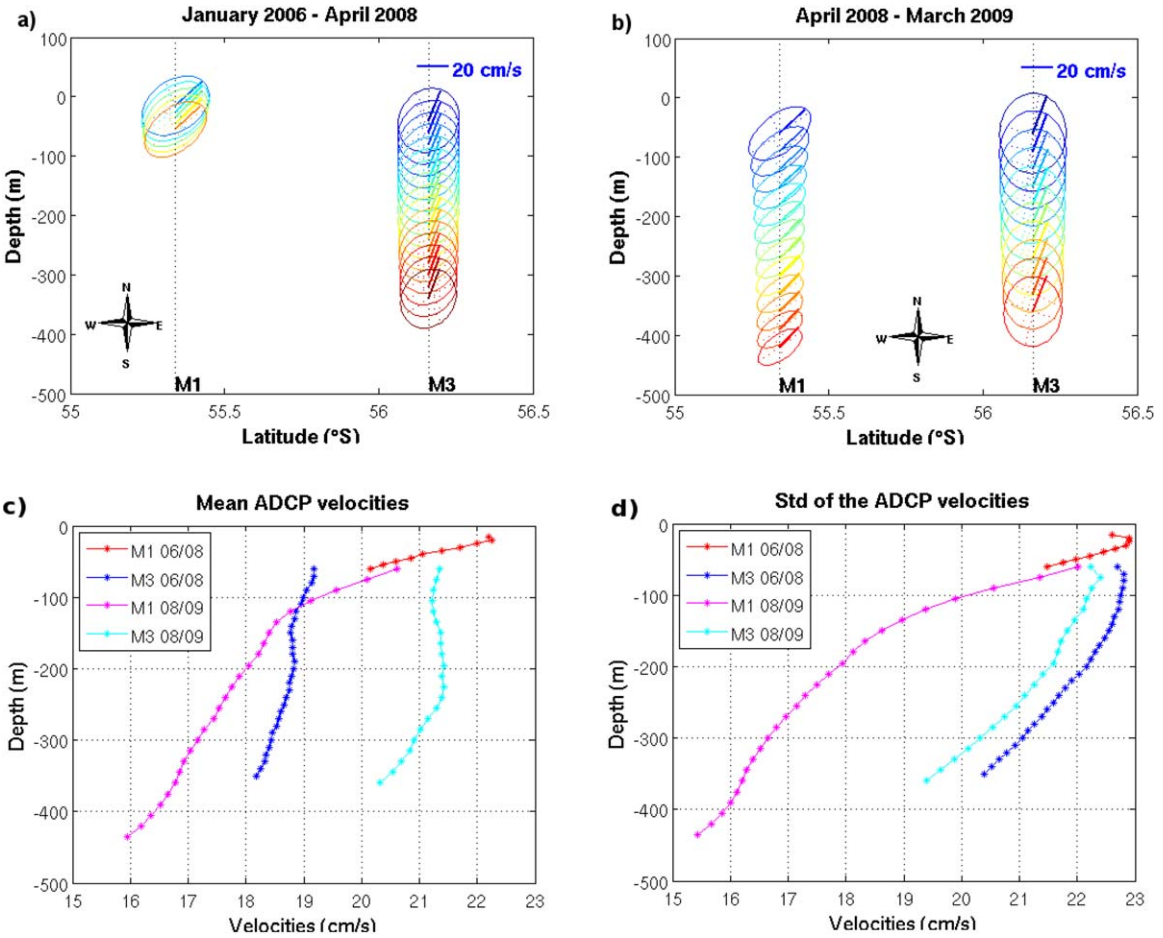

Figure 4. Mean velocities and ellipses of velocity standard deviation at M1 and M3 (from ADCP data) plotted every other depth. (a) Period 2006–2008 (b) Period 2008–2009. Cross-track velocities: (c) mean and (d) standard deviation.

3. Analysis of the Velocities in the Upper 350 m

3.1. The ADCP Data

An ADCP was installed in the uppermost subsurface buoy at M1 and M3. M1 is situated in the steep part of the continental slope of South America and the water depth is around 1500 m. M3 is in the deep part of Yaghan Basin with a water depth of 4250 m (Table 2 and Figure 1). As the moorings were redeployed in April 2008, two profile time series were obtained: from January 2006 to April 2008 and from April 2008 to March 2009 (Figure 3). The vertical resolution is 5 m for M1, 10 m for M3 in 2006–2008, and 15 m for M1 and M3 in 2008–2009. The time step is 2 h for all the time series. The data were daily averaged. M1 2006–2008 profile data are shallow from a nominal depth of 60 m up while the other profile time series extend from 400 m up. Note that the vertical scale varies in Figure 3.

However, on several occasions, particularly at M3, large velocity events ($>$ 80 cm/s) led to spectacular diving of the moorings and to data gaps near the surface (Figure 3, December 2007 at M3 for example). These large velocities were related to the SAF being in a southern location, over M3 (Figure 1). Data gaps near the surface have been filled supposing a null shear above the shallower observation. This hypothesis has a weak influence for M1 2006–2008, M1 2008–2009, and M3 2008–2009 time series which present few gaps in contrast to M3 2006–2008. The gaps in M3 2006–2008 time series are filled with the combination of a no-shear extrapolation (as for the other time series) and a mean shear plus the EOF first mode based on M3 2008–2009, as explained in Appendix A.

The two time series (2006–2008 and 2008–2009) provide similar mean velocity vectors (around 22 cm/s) and standard deviation ellipses (Figure 4). At M1, std ellipses are stretched along isobaths with main axis of

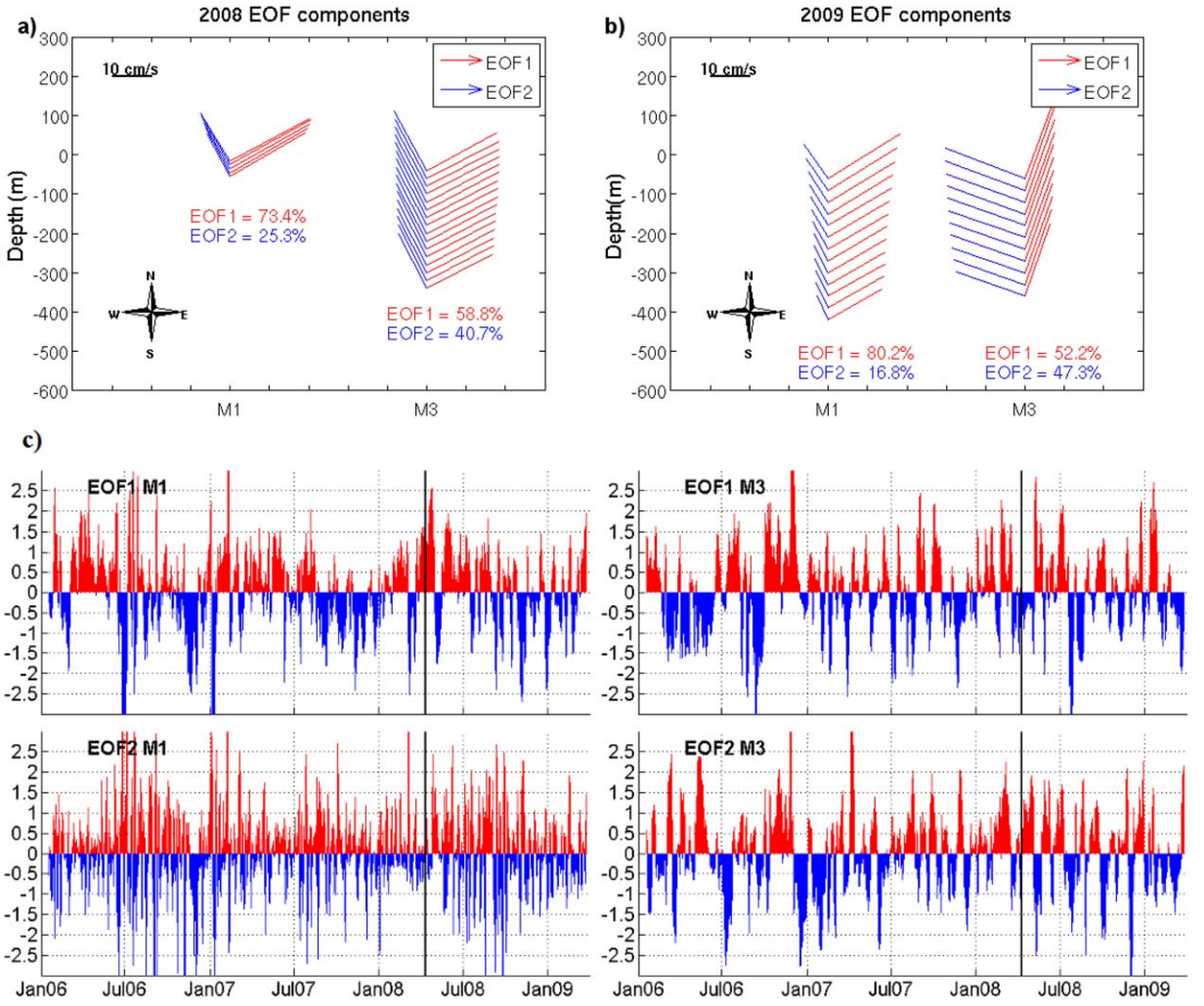

Figure 5. (top) First two principal components of the EOF analysis of the ADCP at each mooring (plotted every other depth). The components are normalized. (a): Period 2006–2008. (b): Period 2008–2009. In red, the first component and in blue the second one. The percentage of explained variance for each component is indicated in the color of the component. We plotted every other depth for more clarity. (c) Temporal evolution of the amplitude of the first two EOFs in 2006–2008 and 2008–2009. The black lines represent the limit between 2006–2008 and 2008–2009 deployments.

the same order as the mean velocity of the corresponding depth. At M3, std ellipses are almost circular, without privileged direction of variation (Figures 4a and 4b). It is probably due to the proximity of the SAF [*Sprintall*, 2003], generating large variations in all directions [*Lenn et al*., 2007]. The mean cross-track velocities show a larger shear at M1 than at M3 (Figures 4c and 4d). Mean cross-track velocities at M3 present a local maximum around 200 m depth also observed in *Firing et al*. [2011] (Figure 4 third transect which is located south of the SAF, as M3). Mean velocities at M1 present a local maximum around 20 m depth. Standard deviations have similar profiles and order of magnitude to mean velocities (Figures 4c and 4d). At M1, cross-track velocity mean and standard deviation do not differ between the two periods (2006–2008 and 2008–2009) (Figures 4c and 4d). At M3, the 2008–2009 mean cross-track velocities are larger by 2 cm/s than the 2006–2008 mean cross-track velocities and the standard deviation differ by 0.5 cm/s (Figures 4c and 4d). Indeed, the SAF is in a northern position during 2008–2009 and there is a higher eddy activity with negative (westward) velocities in 2006–2008 at M3 [*Ferrari et al*., 2012].

3.2. Velocity Variations in the Upper 350 m

An EOF analysis of the four cross-track velocity time series shows that only the first two modes are significant, explaining more than 98% of the variance of each time series (Figures 5a and 5b). The EOF amplitudes slightly decrease with depth without any rotation of the vectors which are orientated northeastward for the

first component and northwestward for the second. The first component at M1 explains more variance than the second one, suggesting more variability in the northeastern direction while the first two components at M3 explain the same amount of variance, indicating an equal variability in all directions, in agreement with the directions and amplitudes observed in *Ferrari et al*. [2012].

M1 EOF components vary at higher frequencies than M3 EOF components (Figure 5c). A wavelet analysis (not shown) highlights the existence of several periodicities at specific moments of the time series. At times, M1 components show energy at an around 10 day periodicity, typical of the Coastal Trapped Waves (CTW), [*Brink*, 1991; *Renault et al*., 2011]; more energy is found in that period in 2006–2008 than in 2008–2009, reflecting a weaker activity of the CTW in 2008–2009. The 30–60 day period, typical of the mesoscale variability [*Ferrari et al*., 2012], has energy in M3 EOF components. Energy is also present at the annual and semiannual periods in the first component of the four time series (M1 and M3 2006–2008 and 2008–2009). These periodicities are often found in the Southern Hemisphere and may be caused by Rossby Waves propagation. These phenomena will be explored further in a companion paper.

The cross-track velocities within the upper 350 m are now used in the construction of the look-up table B defined in section 2.2 (see section 4.1.3).

4. Three Years of Cross-Track Velocities Along Track 104: Method and Validation

The method defined in section 2.2 requires a look-up table of cross-track velocity profiles and an accurate cross-track mean surface velocity. The look-up table is constructed in three steps: first, in the 350–3000 m layer using the cross-track velocities from the current meters; second, in the upper 350 m layer using the ADCP observations and last performing finer interpolations of the table in vertical and along-track directions (section 4.1). A mean cross-track surface geostrophic velocity is then adjusted using an iterative error/correction method (section 4.2), followed by validation of the method against independent data (section 4.3).

4.1. Construction of the Binned Cross-Track Velocity Profiles Along Track 104: A Look-Up Table

4.1.1. Estimates of the Binned Cross-Track Velocity Profiles in the 350–3000 m Depth Range From Current Meters

Cross-track velocity profiles from each mooring are binned into different classes according to the upper current meter velocity. The affiliation of a profile (velocities at three depths in general) to a class is determined by the upper in situ cross-track velocity (60 m for M1 and 350 m for M3 corresponding to the ADCP levels used in *Ferrari et al*. [2012]; otherwise the upper current meter). Ranges for the upper cross-track velocities are chosen so as to get a statistically significant number of data. The selected velocity ranges are: 0–5, 5–10, 10–20, 20–30, 30–40, and larger than 40 cm/s, as well as the opposite intervals for the negative velocities (Figure 6). Two velocity classes are added at M2 because of its location in the SAF: 40–50 cm/s and larger than 50 cm/s (no velocities larger than 60 cm/s are observed at M2, Figure 6). All the intervals are not represented at each mooring: for example, there are no large negative and positive velocities in the Ona Basin (Figure 6, M7). Cross-track velocities at M9 and M10 are pooled together in order to achieve a significant vertical sampling (the three current meters at M10 never recovered data at the same time, and there are only two current meters at M9). For each mooring, this classification provides the dots at the current meter depth in Figure 6.

The class occurrences vary with moorings (Figure 6, color code). Some moorings present a clear dominant class (the 10–20 cm/s class has an occurrence of 20% at M6 for example) and some moorings are lacking a class (for example M7 does not have any near surface velocities in the range 20–30 cm/s and 30–40 cm/s). The occurrence of classes with negative surface velocities is always below 10% as the ACC flow is mainly eastward.

A continuous vertical structure (from 3000 to 350 m) is then obtained by fitting an exponential function on the mean velocities of a given class at the current meter depth (dashed lines in Figure 6). The exponential provides the best fit for all classes of all moorings as a group compared to power, logarithm, and square functions. The major part of the correlation coefficients is larger than 0.80. The fit is very satisfactory for surface velocities less than 20 cm/s ($r > 0.95$). The smallest correlation coefficient (still 0.70) is found at M6 for the class of surface velocities larger than 40 cm/s. The best fit e-folding length scale varies and is in general larger with smaller surface velocities. To improve the regression and better fit the deeper current meter, a

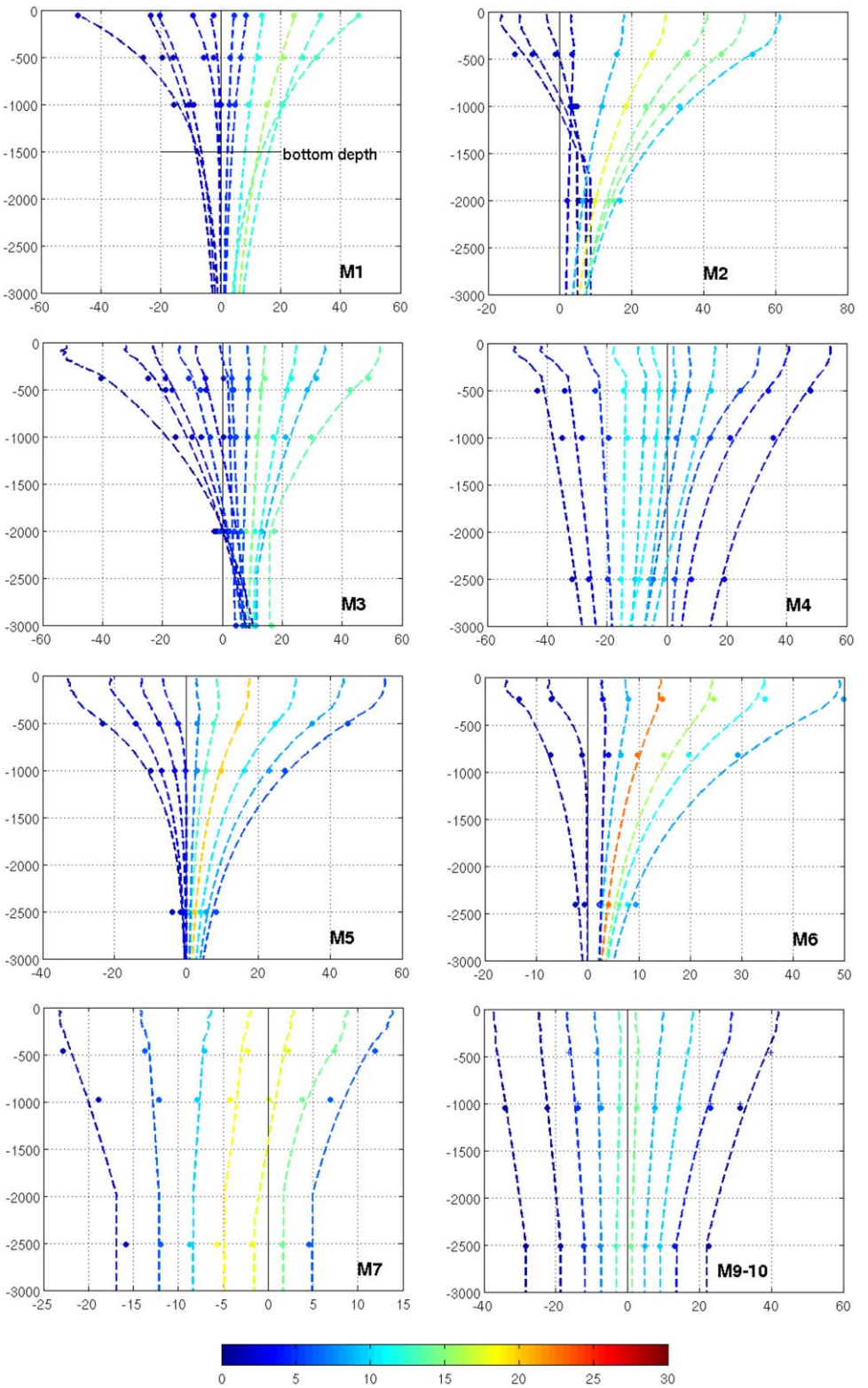

Figure 6. Classes of velocity profiles at the moorings as a function of surface velocity. *X* axis is the velocity (cm/s), *y* axis is the depth (m). The dots are the mean velocities of the current meters for a given surface velocity range. M9 and M10 are considered together. The dashed curves are reconstructed velocity profiles. Colors represent the percentage of occurrence of the class in the time series.

Table 3. Mean and Standard Deviation (std) of In Situ and Reconstructed Velocity Profile Time Series at the Location and Depth of the Current Meters[a]

		Mean				Std				
Moorings	Depth	In situ	MDT09	MDT13	MSGV	In situ	MDT09	MDT13	MSGV	R
M1	20	21.9	21.1	26.3	22.1	17.6	12.8	12.8	12.8	0.78
	60	20.1	18.7	23.5	19.7	18.1	10.7	10.7	10.7	0.77
	500	15.9	15.0	18.5	15.7	14.2	8.1	7.7	8.1	0.77
	1000	11.6	11.9	14.4	12.4	10.8	6.1	5.5	6.0	0.76
M2	450	32.5	28.6	27.4	32.1	15.0	12.8	12.8	12.8	0.89
	1000	21.6	19.7	19	22.0	9.6	8.2	8.3	8.1	0.84
	2000	11.6	10.0	9.7	11.0	8.2	3.8	3.8	3.5	0.58
M3	60	20.9	18.7	18.4	22.0	20.9	18.6	18.6	18.6	0.84
	380	20.1	17.3	17.1	20.2	20.4	16.1	16	16.1	0.85
	500	19.3	16.6	16.5	19.4	17.9	13.3	13.3	13.3	0.85
	1000	15.0	13.6	13.5	15.5	12.5	10.4	10.3	10.3	0.78
	2000	9.5	9.7	9.7	10.5	9.3	5.5	4.6	4.5	0.59
	3000	10.8	8.9	9.0	9.6	9.3	3.1	3.0	3.0	0.45
M4	500	−1.5	5.6	2.0	−1.6	15.0	14.4	14.4	14.3	0.85
	1000	−3.6	2.3	−0.5	−3.4	11.8	11.4	11.6	11.8	0.85
	2500	−8.6	−4.8	−6.3	−7.8	8.9	6.9	7.1	7.5	0.72
M5	500	15.6	21.3	17.2	15.9	12.7	12.9	12.8	12.7	0.91
	1000	9.1	12.4	9.9	9.1	7.5	8.1	8.0	7.9	0.86
	2500	2.1	2.9	2.3	2.1	2.9	2.1	2.0	2.0	0.64
M6	235	21.2	21.2	24.5	21.3	14.7	14.3	14.3	14.3	0.9
	820	13.3	14.2	16.3	14.3	8.3	8.9	8.8	8.9	0.92
	2410	5.1	4.4	4.9	4.4	4.1	2.1	2.0	2.1	0.7
M7	460	0.3	0.5	0.3	0.3	7.3	6.4	6.4	6.4	0.89
	980	−1.8	−0.6	−0.8	−0.8	6.1	5.4	5.5	5.4	0.84
	2515	−3.7	−2.1	−2.3	−2.3	6.1	4.7	4.7	4.7	0.78
M9	1045	3.1	3.9	4.5	3.2	10.5	6.4	6.3	6.4	0.76
	2510	0.7	1.9	2.4	1.4	8.6	4.7	4.6	4.7	0.7

[a]Velocities (mean and std) are in cm/s and the depths of the moorings are in meters. In situ: observed velocities by the current meters. MDT09 (MDT13): velocities calculated using the absolute geostrophic surface velocities obtained from the CNES-CLS09 MDT (CNES-CLS13 MDT). MSGV: velocities calculated using the new mean surface geostrophic velocities determined in this paper. The last column is the correlation (noted R) between the weekly averaged observed velocity time series and the reconstructed ones. They are similar for the three reconstructed velocity time series. Std of in situ velocities are calculated with weekly averaged data.

few velocity profiles are supposed constant below a certain depth: for example 2000 m in M7, 2500 m in M3 when surface velocities exceed 30 cm/s (Figure 6).

4.1.2. Estimates of the Binned Cross-Track Velocity Profiles in the Upper 350 m From ADCP

ADCP data are first binned into different classes according to the velocity at 350 m. Then, the binned upper layer velocity profiles are estimated at each mooring using the ADCP data available from 350 to 15 m. At M1, they are estimated with the ADCP data at M1. M2, M3, M4, M5, and M6 surface shears are filled with the ADCP data of M3 from 350 to 60 m, and with a zero shear from 60 m to the surface. At M7 and M9–10 in the southern Ona Basin, shears in the upper 350 m are estimated using LADCP data from the Ona Basin acquired during the deployments and recoveries of the moorings [*Renault et al*., 2011]. The few available LADCP profiles are then classified depending on the surface velocity, so that the shear depends on the surface velocity. The shear in the upper 350 m is close to zero in the Ona Basin (Figure 6).

Other approaches tested for the binned vertical profiles in the upper 350 m layer yielded less satisfactory results. Comparison with M1, M3, ADCP data, and LADCP transects showed that extrapolation up to the surface of the exponential function obtained from the deep current meter data resulted in overestimation in subsurface shears thus in too large surface speeds. In contrast, a barotropic assumption for the upper 350 m velocities underestimated the subsurface shears in the Yaghan Basin.

Accordingly, classes of velocity profiles with a 10 m vertical resolution have been constructed at each mooring (Figure 6). The binned vertical velocity structures obtained for each mooring as a function of surface velocity show that the amplitude of the vertical shear increases with the amplitude of surface velocity (Figure 6). Globally, there is symmetry between negative and positive velocity profiles, except at M2, M3 (M4) where several profiles with negative (positive) velocities near the surface and positive (negative) velocities

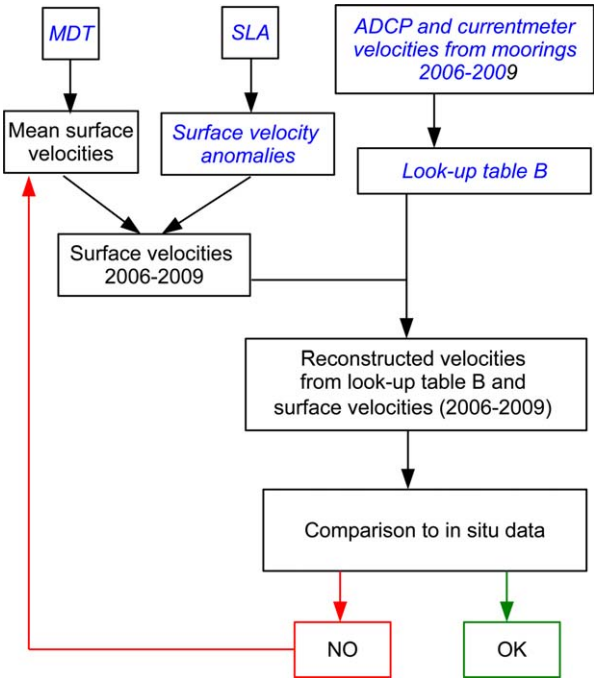

Figure 7. Iterative method used to estimate the new mean surface geostrophic velocities at the mooring points (cf. section 4.2). The mean cross-track surface velocities (MSGV) are adjusted (red arrow) so that the reconstructed velocities fit the in situ data: $MSGV_{new} = MSGV_{old} - (V_{reconstructed500} - V_{insitu500})$. The variables in blue italic are not changed during the iterations.

at depth correspond to the deep cyclonic recirculation in the Yaghan Basin. M7 is symmetric around a negative barotropic reference velocity.

4.1.3. Interpolation: Construction of the Extended Look-Up Table B

All the profiles of Figure 6 are pooled to compose a matrix $B_0(N_x, N_z, N_v)$ with $N_x = 8$ (the eight moorings), $N_z = 451$ (depth from 0 to 4500 m, with a 10 m resolution) and $N_v = 12$ (the number of surface velocity classes varies with sites from 7 to M7 to 12 at M4, Figure 6).

Then, two linear interpolations are successively performed. The first interpolation on the velocity provides a matrix $B_1(N_x, N_z, N_v)$ with $N_x = 8$, $N_z = 451$ and $N_v = 201$. Velocities are interpolated with a step of 1 cm/s from −100 to 100 cm/s. The linear extrapolation out of the observed range was checked to be consistent with the extreme velocity values observed in independent LADCP data (section 4.3). The second interpolation on the distance x along the track with a step of 5 km leads to a matrix $B_2(N_x, N_z, N_v)$ with $N_x = 160$, $N_z = 451$ and $N_v = 201$. This way, the look-up table of velocity profiles along track 104 is constructed.

4.2. Internal Consistency of the Method and Adjustment of the Mean Surface Velocity

Cross-track velocities have been reconstructed along track 104 using the absolute geostrophic surface velocities calculated from the MADT deduced from the CNES-CLS09 MDT or the CNES-CLS13 MDT, and the look-up table created in section 4.1. These velocities averaged weekly have been compared to the velocities observed by the current meters during 2006–2009 (Table 3). Standard deviation of the reconstructed velocities (with a 7 day resolution) is smaller than that of the in situ data (weekly averaged). The satellite data are smoothed due to the processing involved in the computation of the gridded product whereas the in situ data are point measurements. Correlations between the reconstructed and the in situ velocity time series at each depth are above 0.75 at 1000 m for all moorings, with a maximum of 0.92 at M6 (820 m). The deep correlations are larger than 0.58 for all moorings, except at M3 where the correlation at 3000 m is 0.45, which is still a significant value (at the 95% confidence level).

Differences between mean in situ and reconstructed velocities reach 4 and 6 cm/s at M2 (500 m) and M4 (500 m) (Table 3). Even if the CNES-CLS13 MDT performs globally better than the CNES-CLS09 MDT (particularly at M4, M5, and M7), an error in the mean geostrophic surface velocities of a few cm/s will impact transport estimates due to its propagation on the vertical velocity profile, which calls for new mean cross-track surface velocities.

New mean cross-track surface velocities $V_m(x, 0)$ have been estimated at each mooring location to better fit the mean in situ velocities using an iterative procedure schematized in Figure 7. The reconstructed velocities $V(x, z, t)$ using surface velocities $V(x, 0, t)$ (the sum of the new mean cross-track velocities $V_m(x, 0)$ and cross-track velocity anomalies $V'(x, 0, t)$ deduced from the SLA) and the look-up table B are considered good when the difference between the mean in situ velocities at the first current meter (around 500 m) and the mean estimated velocities at the same depth is less than 0.5 cm/s. This successive error/correction method is applied iteratively at each mooring, until the above criterion is verified (Figure 7). Six iterations at most are found to be necessary to provide new cross-track mean surface velocities at the mooring locations

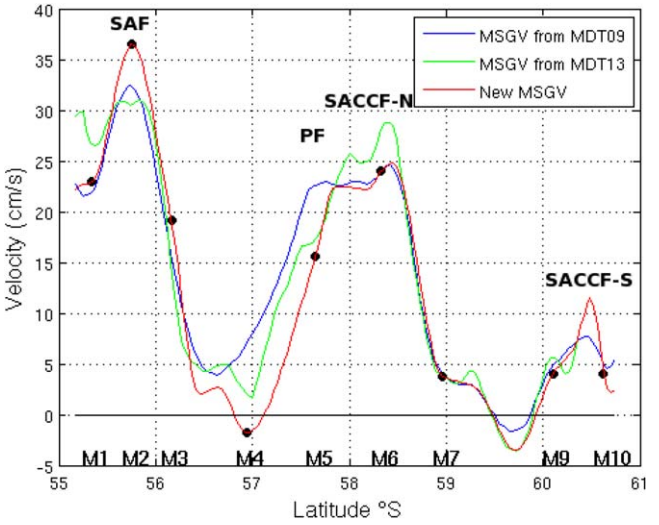

Figure 8. Across-track surface geostrophic velocities deduced from the CNES-CLS09 MDT in blue (MSGV09), and from the CNES-CLS13 MDT in green (MSGV13). Black dots are the mean surface velocities at the mooring locations obtained from the iterative method described in Figure 7. Those points and the cross-track surface velocities derived from the MDTs are used to create the new cross-track mean surface geostrophic velocities (New MSGV) (in red).

(black dots in Figure 8). Along track 104, the new mean surface velocities are adjusted to fit the new estimate at the mooring locations and conserve the trend deduced from the CNES-CLS09/13 MDT between moorings (Figure 8). The new mean surface velocities present a stronger SAF and an intensified recirculation around 57°S. In the Ona Basin, velocities are kept close to mean velocities obtained from the CNES-CLS13 MDT which captures the recirculation.

Velocities reconstructed using the look-up table B and the new cross-track velocities are compared to the current meter data (Table 3). Reconstructed mean velocities are in agreement with the in situ velocities, with differences of less than 1.5 cm/s at all depths. Results are particularly satisfying at M5 and M2. These reconstructed velocities explained more than 75% of the variance at the upper current meter and more than 45% of the variance at the lower current meter. The explained variance at the upper current meter at M1 is smaller (60%) because of the 7 day resolution surface velocities that miss the high frequency signals along the northern slope (topographic waves for instance) mentioned in section 3.2.

Comparisons have also been done with the bottom cDrake current meter close to M4 at 4100 m depth and 50 m from the bottom [*Chereskin et al*., 2009; *Firing et al*., 2014]. The correlation is satisfying (0.42). Hence the reconstructed velocities deduced from the altimetric data using the new mean surface velocities and the look-up table are satisfactory at the mooring locations.

4.3. Comparison With Independent Data: Geostrophic Velocities Referenced to LADCP

The calculated velocities using the look-up table B and the new mean surface velocities presented in the previous subsection are compared to geostrophic velocities derived from CTD data referenced to LADCP data [*Renault et al*., 2011], named LADCP adjusted geostrophic velocities hereafter. The two transects of 2006 were performed within 3 weeks (first transect: 16–26 January, second transect: 31 January to 6 February) and have a horizontal resolution of 20 km between stations (similar to the resolution of altimetric maps) and a vertical resolution of 10 m (similar to the look-up table). The second transect is not complete and stops at 60°S.

The major features observed in the LADCP adjusted geostrophic cross-track velocities (Figures 9a and 9b) are from north to south: the strong eastward flow of the SAF, a strong cyclonic eddy centered at 56.4°S (labeled N2 as in *Renault et al*. [2011]), the PF centered at 57.5°S, the northern branch of the SACCF (SACCF-N) centered at 58.4°S, an anticyclonic eddy (labeled P10 as *Renault et al*. [2011]) centered at 59.5°S, and the southern branch of the SACCF (SACCF-S at 60.5°S). The position, intensity of the fronts, and the eddies evolve between the transects, with for example eddy N2 advected to the southeast leaving the section, negative velocities appearing between the PF and SACCF-N, and P10 weakening [*Provost et al*., 2011]. The reconstructed velocity sections (Figures 9c–9f) present the fronts (the SAF, the PF, and the two branches of the SACCF) and the two eddies. The evolution between the reconstructed transects matches those observed in the two LADCP transects.

The cumulated transports over 3000 m and from the surface to the bottom are shown in Figure 10 and Table 4. Total transport over 3000 m is 134 Sv for the LADCP adjusted geostrophic velocities (transect 1),

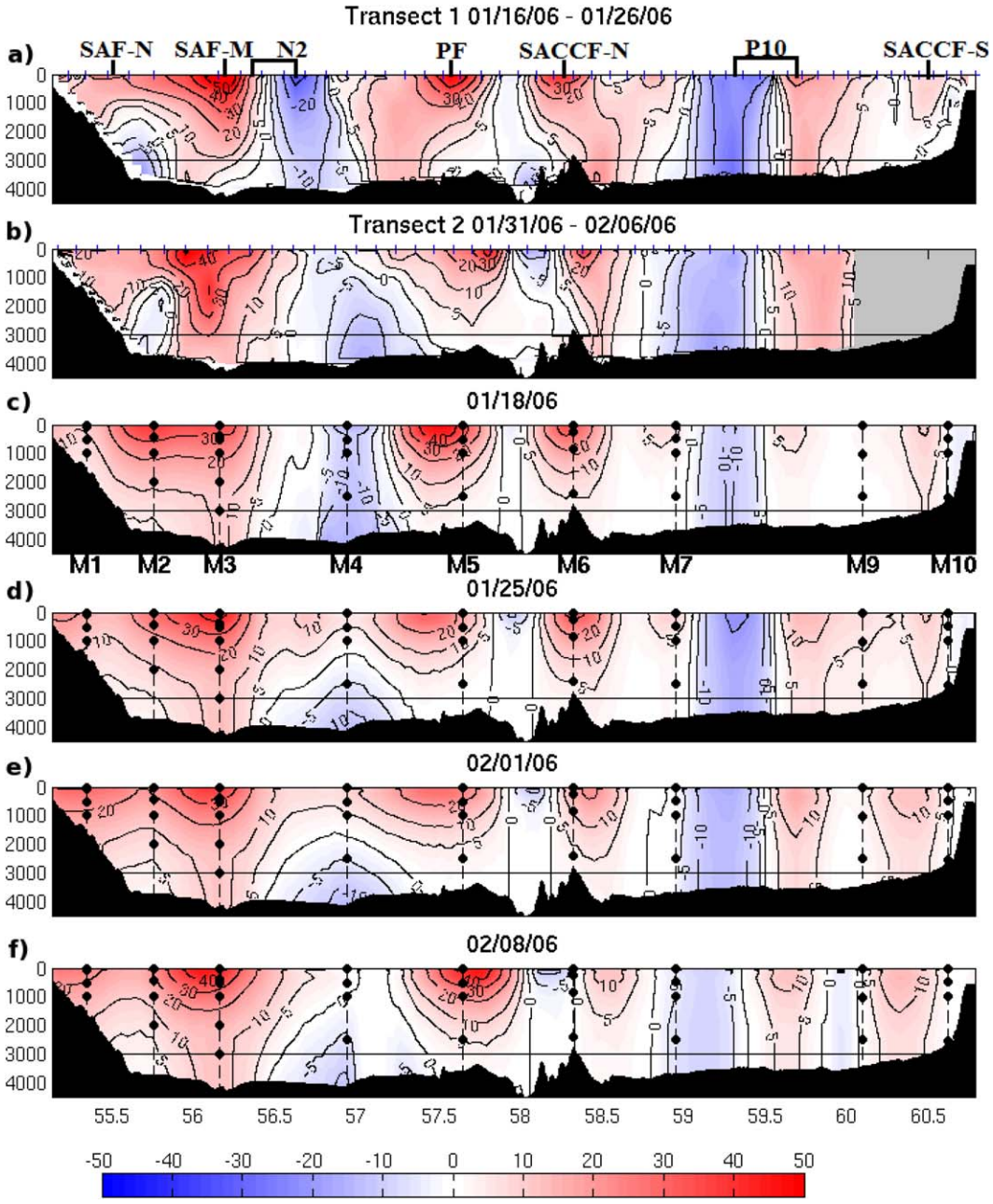

Figure 9. (a) Geostrophic velocities from the transect 1: 16 January 2006 to 26 January 2006. (b) Geostrophic velocities from the transect 2: 31 January 2006 to 6 February 2006. Note that this transect stops at 60°S. (c), (d), (e), and (f) Velocities deduced from the look-up table and altimetry for the four nearest date of the LADCP transects: 18 January 2006 (c), 25 January 2006 (d), 1 February 2006 (e), 8 February 2006 (f). The ticks in plot (a) and (b) are the locations of the LADCP/CTD stations. Black dots are the positions of the current meters. Bathymetry is shown in solid black. Velocities (colorbar) are in cm/s. *x* axis is latitude (° S) and *y* axis is depth in meter.

136 and 140 Sv for the reconstructed velocities of the first and second week, respectively (Figures 9c and 9d). Cumulated transport over 3000 m at 60°S for the second transect is 117 Sv and cumulated transport at 60°S for the reconstructed velocities of the third and fourth week (Figures 9e and 9f) are 124 Sv. *Renault et al*. [2011] estimated the uncertainty bars on the transport evaluations from the in situ data as 7 Sv. Therefore, reconstructed transports at the nearest satellite dates fall within the error bar of the transport estimated from the in situ data.

Full-depth transports and transports above 3000 m differ only by 1 Sv in the LADCP adjusted geostrophic velocities (for both transects, Table 4). In the reconstructed velocities at these dates, transports between

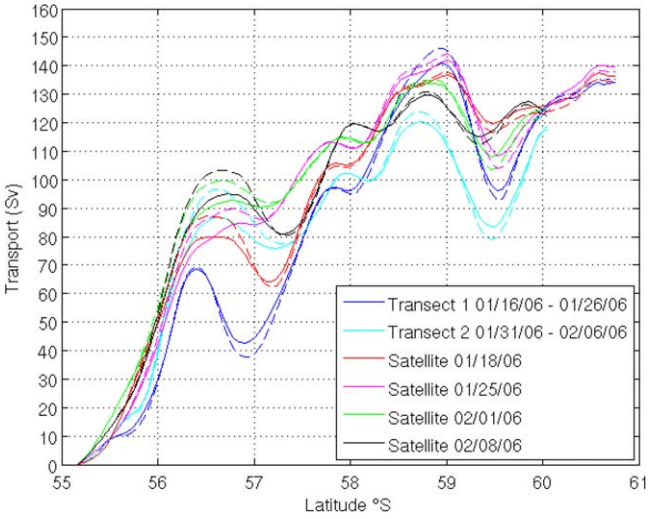

Figure 10. Cumulated transport. Solid lines: cumulated volume transport over 3000 m for transect 1, 2, and the four nearest satellite dates. Dashed lines: cumulated volume transport over the whole water column (surface to bottom). Note that the transports from the reconstructed velocities are within the error bar of the LADCP-adjusted geostrophic velocity transport: 7Sv [*Renault et al*., 2011]. See values in Table 4.

3000 m and the bottom is less than 3 Sv. Differences between the cumulated transport over 3000 m and bottom-surface are noticeable in the areas of large velocities (fronts and eddies) and cancel out in each basin (Figure 10 comparing dashed and full lines of the same color). The small transport values below 3000 m result from the topography: the deep local circulation cells in the two semiclosed basins have a close to zero net transport as westward and eastward flows tend to cancel out.

The reconstructed velocity transects and derived transports are in good agreement with those derived from the in situ data, which is remarkable considering the difference in time resolution and the rapid evolution of the flow [*Barré et al*., 2011]. In particular, all transport estimates from reconstructed velocities fall within the error bar (±7 Sv) of the in situ estimates. We now examine the structure of the mean and standard deviation of the reconstructed cross-track velocities over the 3 year observation period.

4.4. Mean and Standard Deviation of the Reconstructed Cross-Track Velocities Over 2006–2009

The mean and standard deviation of the reconstructed cross-track velocities over the observation period (Figure 11) are consistent with the in situ observations at the mooring sites [*Ferrari et al*., 2012, 2013] and with the satellite observations for the near surface variations [*Barré et al*., 2011]. The reconstructed mean cross-track velocities show three bands of eastward flow extending to the bottom corresponding to the SAF (north of 56.5°S), the PF-SACCF-N (between 57.3°S and 59°S), and the SACCF-S (60.25°S). Westward deep velocities in the center of the Yaghan Basin correspond to the deep recirculation (Figure 11a). The negative velocities around 59.5°S have not been sampled by any mooring and are deduced from the surface velocities. The negative velocities in the Yaghan Basin have already been observed by *Lenn et al*. [2007] and *Firing et al*. [2011].

Velocity standard deviation (std) values vary spatially with, as expected, large values in the upper layer in the Yaghan Basin, in excess of 15 cm/s, and lower values in the Ona Basin, mostly below 10 cm/s (Figure 11b). Surface velocity std shows a local minimum at 56.25°S as dictated by satellite altimetry [*Barré et al*., 2011]. Large upper layer std values are associated with large mean flows. At depth, relatively large std values (6–7 cm/s) are found in the Ona Basin corresponding to the barotropic nature of the flow there. Relatively large std values are observed at depth on the southern edge of the SAF, in the recirculation region and on the northern edge of the PF, around M4, in concordance with the large variations observed in the deep velocities (Figure 6) [*Ferrari et al*., 2012].

Table 4. Total Transport for the Two Transects, and the Four Nearest Satellite Date[a]

	Total	
	0–3000	Full-depth
Transect 1	134 ± 7	135 ± 7
01/18/06	136	134
01/25/06	140	138
Transect 2	117 ± 7	118 ± 7
02/01/06	124	122
02/08/06	124	123

[a]0–3000: transport referenced to 3000 m. Full-depth: transport referenced to the bottom. Note that transect 2, 1 February 2006 and 8 February 2006 stops at 60°S. Transport are in Sv.

5. Volume Transport Through Track 104

The 20 year time series of surface velocities from altimetry were examined to check how representative the 2006–2009 years (used to built the look-up table) were. At any given latitude, the 2006–2009 surface velocities

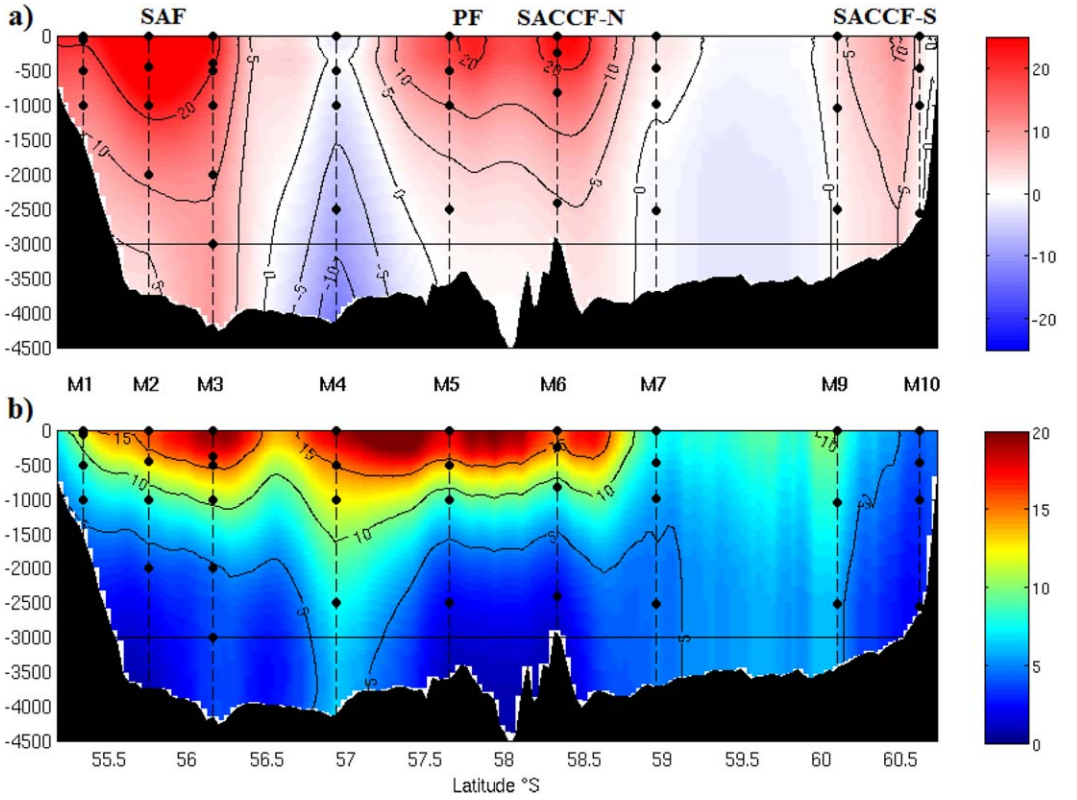

Figure 11. Reconstructed velocities over 2006–2009: (a) mean and (b) standard deviation. Velocities (colorbar) are in cm/s. *x* axis is latitude along track 104 (°S). *y* axis is depth in meters. Bathymetry is shown in solid black. Black dots are the position of the current meters.

sampled the full range of surface velocities encountered in 20 years. The look-up table B created in section 4.1 from the 2006–2009 data were used to extrapolate the volume transport calculation over the 20 years of altimetry.

5.1. Total, Barotropic, and Baroclinic Transport Time Series Over the 20 Years of Altimetry: Mean and Std

The volume transport in the upper 3000 m is estimated using the look-up table and the altimetric time series (1992–2012) (Figure 12a and Table 5, 7 day resolution in dark, smoothed transport with a 1 month running mean in green). The mean transport is 140 Sv, with a standard deviation of 10 Sv (standard deviation of 7.6 Sv for the smoothed transport) and a standard error of the mean of 2.2 Sv. The full-depth total transport has a mean of 141 Sv with a standard deviation of 13 Sv (Figure 12b and Table 5). The mean full-depth transport is only 1 Sv larger than the mean transport in the upper 3000 m, in agreement with the observations made in section 4.3.

Time series of the baroclinic (calculated imposing a zero velocity at the reference level) and barotropic transports over 3000 m and over the whole water column are also shown in Figure 12. The shift of reference level for calculating the barotropic transport leads to a large difference in the mean partition between barotropic and baroclinic transports (Table 5). The mean barotropic transport over 3000 m is 28 Sv with a standard deviation of 12 Sv and a standard error of the mean of 1.6 Sv; the mean baroclinic transport over 3000 m is 112 Sv with a standard deviation of 7 Sv and a standard error of the mean of 1.6 Sv. The full-depth baroclinic transport is 136 Sv and the barotropic one 5 Sv, with std 11 Sv and 16 Sv, respectively. The standard error of the mean is 2.7 Sv for the baroclinic transport and 4.0 Sv for the baroclinic one.

The total transport std is larger than the std of the baroclinic transport and smaller than the std of the barotropic transport. Indeed, the baroclinic and barotropic transports present a large significant (95% level) degree of anticorrelation (−0.5) leading to the total transport having a smaller std than the barotropic

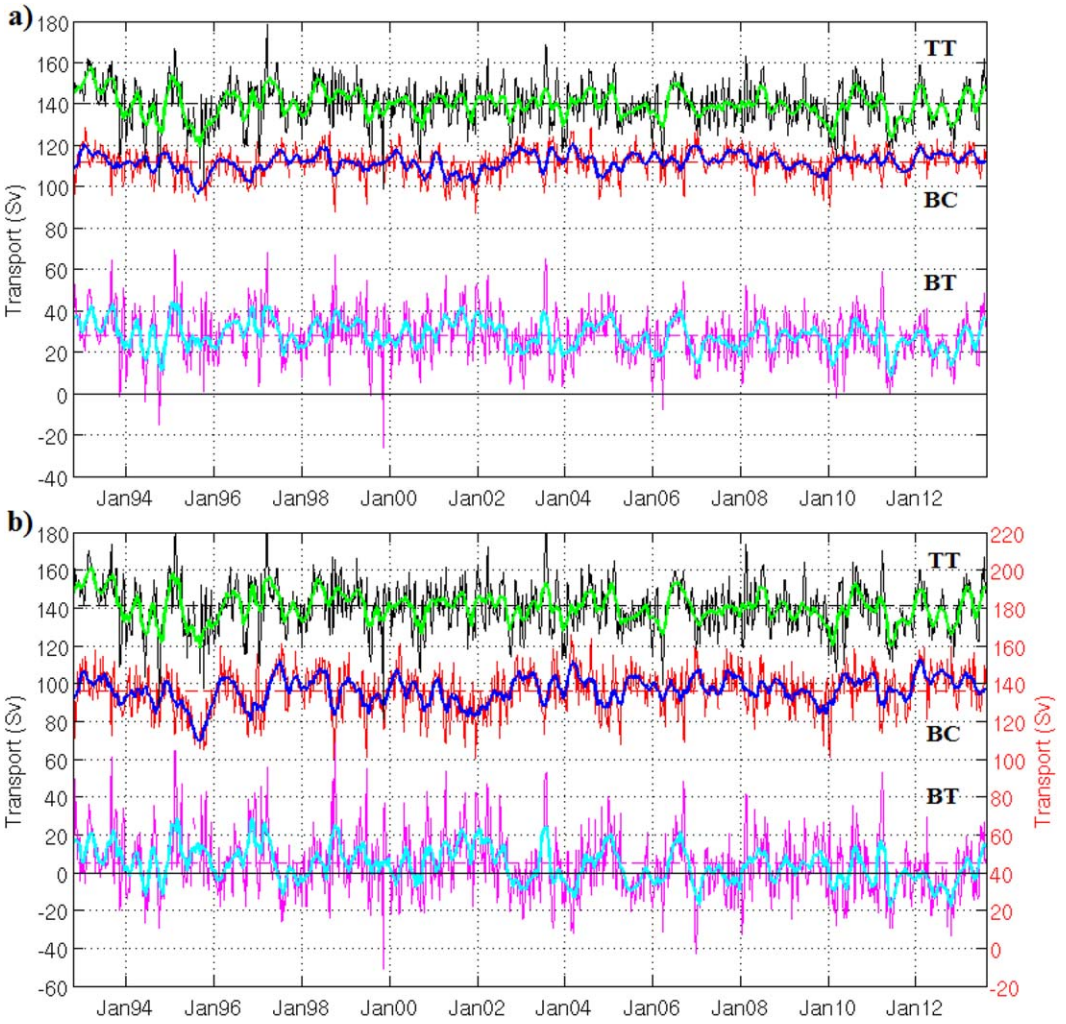

Figure 12. (a) Time series of the total (black), baroclinic (red), and barotropic (magenta) transport above 3000 m, with their smoothed series obtained using an 1 month running mean. Total mean: 140 Sv, std: 10 Sv. Barotropic mean: 28 Sv, std: 12 Sv. Baroclinic mean: 112 Sv, std: 7 Sv; (b) Time series of the total (in black), baroclinic (in red), and barotropic (in magenta) transport from 0 to bottom, with their smoothed time series (respectively green, blue, and light blue) obtained with a 1 month running mean. Total mean: 141 Sv, std: 13 Sv Barotropic mean: 5 Sv, std: 16 Sv. Baroclinic mean: 136 Sv; std: 11 Sv. Note that the red right axis refers to the baroclinic transport only.

transport. As a result, the transport range is 110 Sv for the total transport, 68 Sv for the baroclinic transport, and 119 Sv for the barotropic transport (Figure 12b and Table 5).

5.2. Variations in the Transport Time Series

An important short-term variability is noticeable, with significant variations of more than 25 Sv in less than 4 weeks. For example, at the end of January 1995 to the beginning of February 1995, the nonsmoothed transport increases by 29 Sv (from 139 to 168 Sv) in 4 weeks; by 26 Sv in 3 weeks during September 1995 (from 108 to 144 Sv).

Differences between the annual means of volume transport are indicative of an interannual variability, and the annual standard deviations of an intra-annual variability (Figure 13). Year 1993 is characterized by a large annual mean (150 Sv, standard deviation of 12.6 Sv), 1995 and 2011 by smaller annual means (respectively 134.7 Sv and 133.6 Sv, standard deviations of 17.9 Sv and 12.4 Sv, respectively), whereas 2009 has a small standard deviation (8.8 Sv). The mean annual barotropic transport varies from −6 Sv (2012) to 12 Sv (1993 and 2001) and the std from 17.7 Sv (1995) to 11.1 Sv (2007) (Figure 13). The mean annual baroclinic transport varies from 144 Sv (2012) to 122 Sv (1995) and the std from 8.3 Sv (1992) to 13.4 Sv (1998). As expected from section 5.1, the baroclinic and barotropic annual means are anticorrelated (−0.68).

Table 5. Mean, Standard Deviation (std), Standard Error of the Mean (sem), and Range of the Total (TT), Barotropic (BT), and Baroclinic (BC) Transport Referenced to 3000 m and to the Bottom for the Raw Transports (top) and the Smoothed Transports (bottom) With a 1 Month Running Mean[a]

	Raw Transport					
	TT 3000	BC 3000	BT 3000	TT Full-Depth	BC Full-Depth	BT Full-Depth
Mean	140	112	28	141	136	5
Std	10	7	12	13	11	16
Sem	2.2	1.6	1.6	2.7	2.7	4.0
Range	79	42	95	110	68	119
	Smoothed Transport					
	TT 3000	BC 3000	BT 3000	TT Full-Depth	BC FULL-Depth	BT Full-Depth
Mean	140	112	28	141	136	5
Std	7.6	4.1	6.5	7.6	7.0	9.0
Sem	1.6	1.6	1.6	1.6	1.7	2.3
Range	38	24	36	42	42	47

[a]3000: transport referenced to 3000 m. Full depth: transport referenced to the bottom. Mean, std, sem and range are in Sverdrup.

Slight long-term trends are observed in all raw and smoothed transport time series (Figures 12 and 13). The total volume transport time series shows a weak decreasing trend (between −0.11 Sv and −0.32 Sv per year at a 95% confidence level for the transport above 3000 m and between −0.18 and −0.44 Sv per year

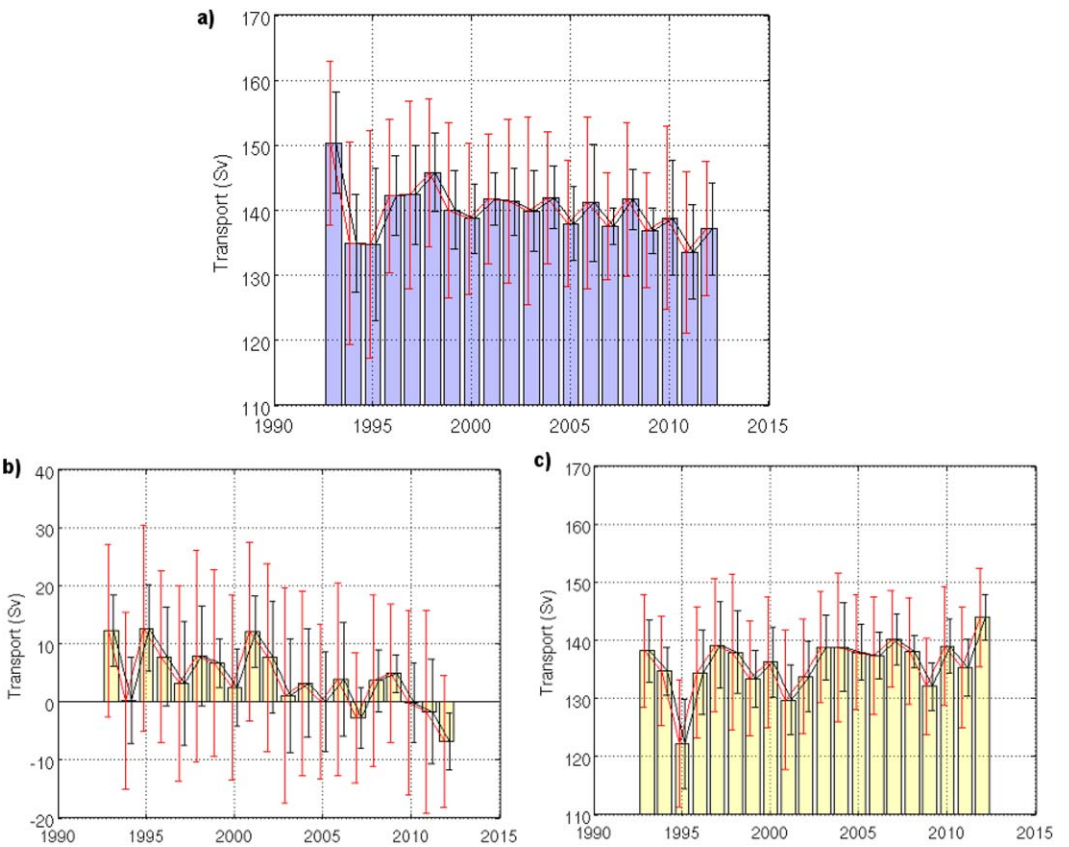

Figure 13. (a) Mean annual transport. In red, the annual std of the time series of the raw transport. In black, the annual std of the time series of the smoothed transport. (b) Mean annual barotropic transport and (c) Mean annual baroclinic transport. (b) and (c) In blue, the annual std of the time series of the raw transport. In black, the annual std of the time series of the smoothed transport.

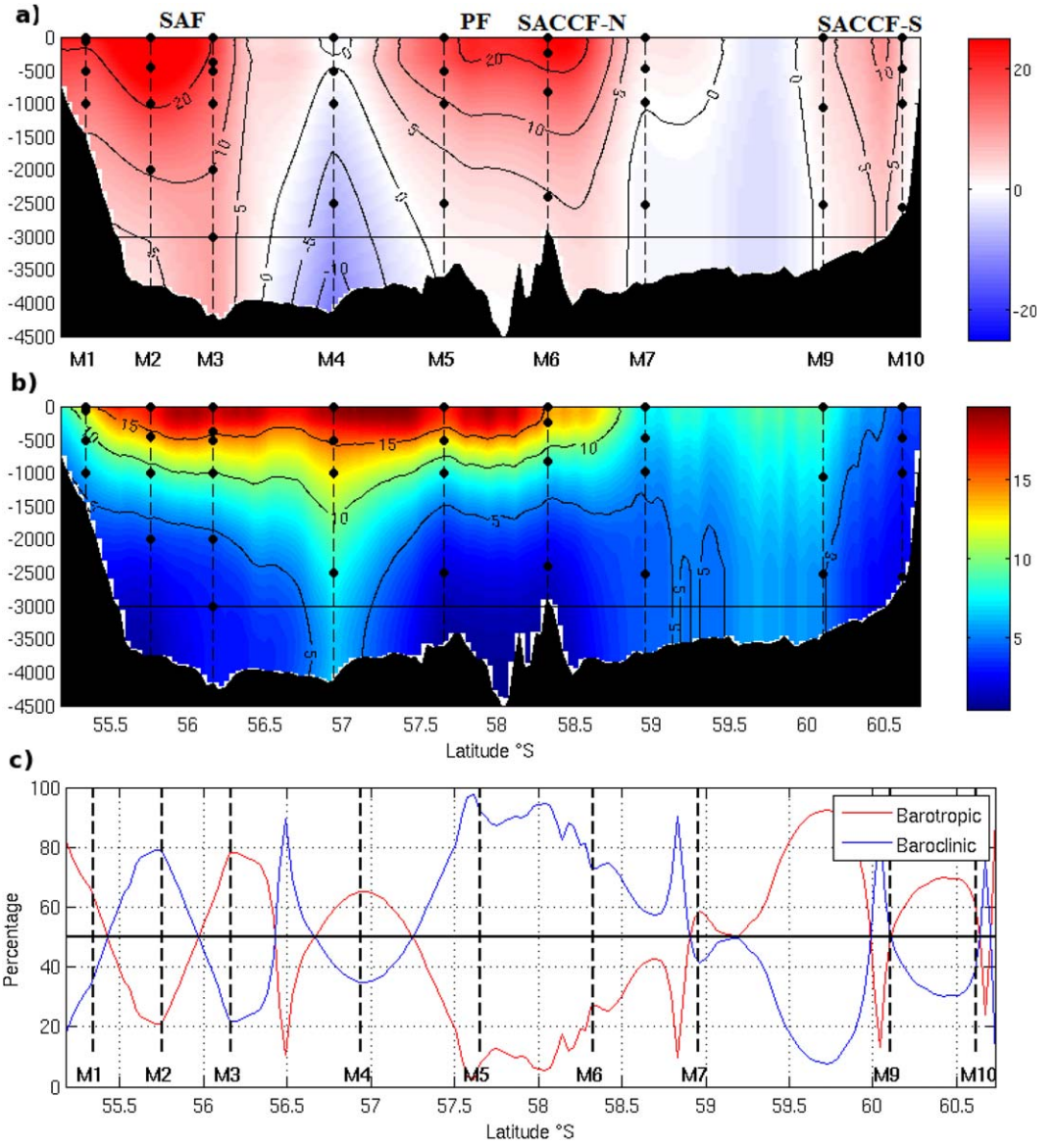

Figure 14. Cross-track velocity profiles in cm/s (a) mean and (b) standard deviation. Black dots are the position of the current meters. Bathymetry is shown in solid black (c) Percentage of the barotropic/baroclinic component over the total transport integrated on the whole water column. In red, the baroclinic component. In blue, the barotropic component.

for the transport from the bottom to the surface). Both barotropic transport time series (above 3000 m and over the whole water column) exhibit a decreasing trend (between −0.23 Sv and −0.47 Sv per year above 3000 m and between −0.44 and −0.77 Sv per year for full depth at a 95% confidence interval). In contrast, the baroclinic time series present a small increasing trend (between 0.07 Sv and 0.2 Sv per year above 3000 m and between 0.23 Sv and 0.47 Sv at a 95% confidence interval). These general trends are small if we consider that the 7 Sv error bar of *Renault et al*. [2011] is valid for this volume transport time series.

5.3. Mean Velocity Distribution Along the Track

The mean and standard deviation of the reconstructed velocities over the 20 years of altimetry (Figures 14a and 14b) are similar to those obtained during the 3 years 2006–2009 and described in section 4.4 (Figure 11). The section of the difference between the two means (not shown) points out small velocity differences of less than 5 cm/s in amplitude corresponding to a slightly stronger SAF further south, a PF further north, a SACCF-N further south, and a slightly weaker SACCF-S in the 3 years sampled with the Drake experiment.

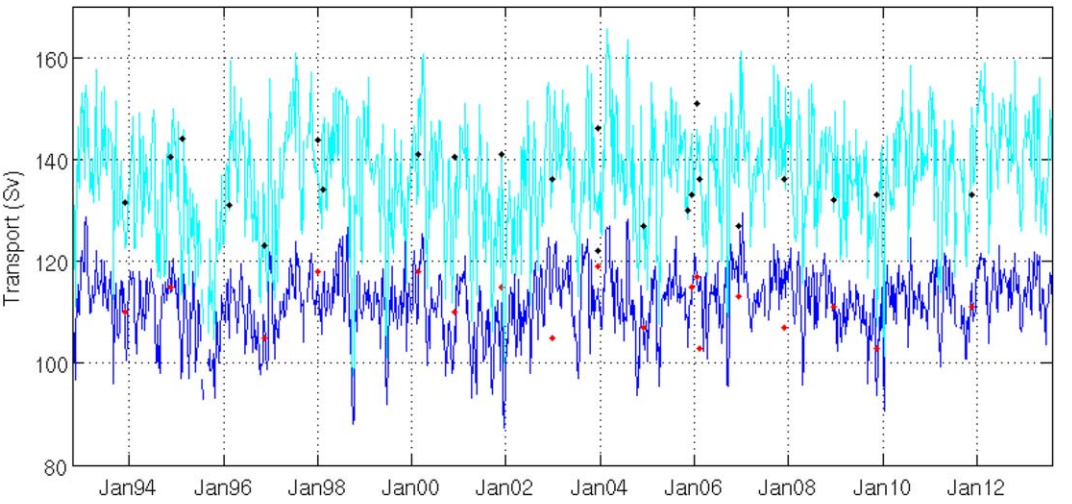

Figure 15. (light blue) Baroclinic transport referenced to the bottom. (dark blue) Baroclinic transport referenced to 3000 m. The dots represent the transport estimates from hydrographic sections in Drake Passage. The dark dots refer to the full-depth baroclinic transport, the red dots to baroclinic transport over 3000 m.

The mean transports estimated during the 3 years of the experiment, 138 Sv for total transport (TT), 136 Sv for baroclinic transport (BC), and 1.8 Sv for barotropic transport (BT), correspond to small values for TT and BT, and an average value for BC in the 20 year long time series.

The contribution of the mean barotropic and baroclinic components to the total transport is calculated as a function of latitude along the track (Figure 14c). As expected, a large mean baroclinic component (more than 80%) is observed near the fronts (SAF around 55.75°S, PF and SACCF-N around 58°S) where upper layer velocities are strong. In the other part of the Yaghan Basin where upper layer velocities are much weaker (near 56.25°S), the barotropic component is largely representative of the total mean (Figure 14c). The barotropic component is important in the Ona Basin around 59.5°S and 60.5°S where velocities are weak. Important barotropic velocities are also observed near the south American continental shore because of the steep topography.

The contribution of the baroclinic and barotropic components to the transport variations, the spectral content of the transport variations, and the potential drivers of the observed variations are analyzed in a companion paper (Z. Koenig et al., manuscript in preparation, 2014).

6. Discussion of the Robustness of the Method

6.1. Baroclinic Transport: Comparison With Estimates From Hydrographic Transects

The baroclinic transport time series is compared to punctual baroclinic transport estimates from several sources in Drake Passage: from the SR1b repeat hydrographic section [*Cunningham et al.*, 2003; *García et al.*, 2002], from Vavilov and Ioffe section [*Koshlyakov et al.*, 2007] and from the LADCP transects along track 104 [*Renault et al.*, 2011]. In all those papers, two baroclinic transports were calculated: one with a reference level at 3000 m, the other with the reference at the bottom. We calculated the baroclinic transport estimates (with reference level at 3000 m and bottom) across the 10 SR1b transects performed from 2003 to 2011.

Both baroclinic transport time series, referenced to 3000 m or to the bottom, fit remarkably well the punctual estimates (Figure 15). First, the punctual baroclinic transport characteristics (mean and std) are comparable to those of the baroclinic transport time series over 1992–2012 (mean 136 Sv, sem 2.7 Sv, std 11 Sv). Indeed, the average baroclinic transport estimated by *Cunningham et al.* [2003] from the six annually repeated SR1b transects from 1993 to 2000 was 136.7 Sv with a standard deviation of 7.8 Sv. The average baroclinic transport calculated here with the 10 SR1b sections from 2001 to 2011 is 134.4 Sv with a standard deviation of 5.8 Sv.

It is noteworthy that there is no significant bias between different estimates. In fact, the mean of the difference between hydrography derived estimates and our transport time series is zero above 3000 m and 1 Sv for the entire water column. Second, the rms difference is 6.4 Sv for the baroclinic transport above 3000 m

Table 6. Mean, Standard Deviation (std) and Standard Error of the Mean (sem) of the Different Volume Transport Time Series Over 3000 m[a]

		MDT09	MDT13	NMSGV
Total	Mean	158	153	140
	Std	10	10	10
	Sem	2.1	2.1	2.2
Barotropic	Mean	37	35	28
	Std	12	12	12
	Sem	1.6	1.6	1.6
Baroclinic	Mean	121	118	112
	Std	7	7	7
	Sem	1.6	1.6	1.6

[a]MDT09/MDT13: transport time series reconstructed using the surface geostrophic velocities derived from the CNES-CLS09 MDT/CNES-CLS13 MDT. NMSGV: transport time series reconstructed using the new mean surface geostrophic velocities derived from the error/correction method shown previously. Transport, Std, and SEM are in Sverdrup.

and 10.5 Sv for the full-depth baroclinic transport. The values of baroclinic transport time series at the dates of the transects fall within the error bars of the transect estimates, which vary from 7 Sv [*Renault et al*., 2011] to 15 Sv when the station spacing is great.

6.2. Sensitivity to the Mean Dynamic Topographies

We compared the volume transport calculated using the new mean surface velocities (elaborated in section 4.2) with that using surface mean velocities derived from the CNES-CLS09 and CNES-CLS13 MDTs. The long-term trends, standard deviations, and the spectral content of transports (not shown) do not show any significant change. On the other hand, the mean transport changes significantly: it increases from 140 Sv from our method to 158 Sv with the CNES-CLS09 MDT and 153 Sv with the CNES-CLS13 MDT (Table 6). This is consistent with *Griesel et al*. [2012] who remarked that the use of the CNES-CLS09 MDT for transport computation leads to an overestimation of the volume transport. They attribute it to a lack of mass conservation in the production of the MDT. The same issue is also encountered with the CNES-CLS13 MDT. In fact, the two MDTs exhibit too large velocities between the SAF and PF (56.5–57.5°S) compared to our best estimates (Figure 8).

Barotropic and the baroclinic transports differ from the values calculated with the adjusted mean surface velocities by about 9 Sv while their standard deviations remain the same (Table 6). Note that the mean barotropic and baroclinic transport contribute about 20 and 80% to the total transport, respectively.

6.3. A Posteriori Comparison With the "Classical" Method

The "classical" method requires the estimates of the mean velocity $V_m(x, z)$ and a correlation $A(x, z)$ between velocity at depth z and surface velocity (section 2.2). Both $V_m(x, z)$ and $A(x, z)$ are independent of time and the velocity time dependence should be provided by the altimetry derived surface velocity anomalies. The a posteriori comparison between the "new" method and the "classical" method is detailed in Appendix B. As $V_m(x, z)$ and $A(x, z)$ could not be extended across Drake Passage from only nine moorings, the new method was developed (section 2.2).

In the "new" method, the correlation between velocity at depth z and the surface velocity is not constant a priori. The a posteriori estimated time mean and standard deviation of A show that the new method exhibits coherent results compared to the classical method. Transport estimates using the mean function $A(x, z)$ and the mean velocity $V_m(x, z)$ are close to the transport from the new method (difference of 2 Sv in the mean).

6.4. Methodological Errors

It is difficult to estimate the methodological error caused by the horizontal and the spatial sampling from in situ data. A sensitivity study was performed using the Orca 12 model outputs from 2006 to 2009 (1/12° horizontal and 3 day temporal resolution) (www.mercator-ocean.fr/eng/science/composantes-systemes/modelisation/orca12). Although a general good agreement is observed between the model outputs and the in situ data from the moorings (R. Ferrari et al., Heat fluxes across the antarctic circumpolar current in drake passage: Mean flow and eddy contributions, submitted to *Journal of Geophysics Research: Oceans*, 2014), the differences between the model cross-track velocities and the current meter cross-track velocities put a stringent limit on the exercise of improving the error analysis using the model. Mean model cross-track velocities are larger than mean in situ velocities. The standard deviation of the model cross-track velocities in the upper 1000 m is larger than in the model outputs.

We built up a look-up table B′ using velocity time series at the depth and locations of the in situ observations. We reconstructed the velocity field along the section using this look up table and the model cross-track near surface velocity. The rms difference between the reconstructed transport and the model transport was 11 Sv.

Wavelet analyses showed that the two time series (model transport and reconstructed transport) are in phase (zero-lag) with coherences constantly above 0.75 for time scales larger than 3 months.

We built another look-up table adding four moorings (between M3 and M4, M4 and M5, M5 and M6 and M7 and M9). The rms difference and the coherences between the reconstructed and model transports remained the same. It seems that the in situ moorings caught the major structure of the cross-track flow and allowed, in combination with altimetry, a satisfactory estimate volume transport time series. This 11 Sv should be considered as an upper bar of uncertainty, since the comparisons with independent in situ data (Drake hydrography from *Renault et al*. [2011], baroclinic transports from SR1b) or with the classical method (see appendix B), showed an uncertainty around 7 Sv.

6.5. Limitations

A posteriori comparisons with independent data sets such as the Drake Hydrography LADCP transects from *Renault et al*. [2011] or the baroclinic transport estimates from the repeated SR1b section [*Cunningham et al*., 2003] are very satisfying. The altimetry derived transport estimates showed no bias and fell within the error bars of the in situ estimates: the method is robust.

Adjustment of the mean surface velocities provided excellent agreement between the reconstructed velocities and the in situ observations in the upper 3000 m (Table 3). The remarkable agreement with the cDrake current meter data near the bottom at M4, and the reasonable a posteriori check of a close to zero net flow between 3000 m and bottom make the extrapolation from 3000 m to the bottom less risky even if the look-up table was constructed with no data below 3000 m. Indeed, the time series of transport between 3000 m and the bottom (not shown) has a mean of 0.6 Sv, a std of 3 Sv, and a range of 30.4 Sv. This part is noisy, explaining the std difference between the full depth and 0–3000 m total transport (Table 5).

Altimetry products used in the reconstruction of the velocity fields have a 7 day resolution, and cannot fully resolve high-frequency variations on the slopes (Coastal Trapped Waves for example). Correlations are somewhat smaller at the extremities of the sections at M1 and M10, although they still are well above 0.7 (Table 3). There is certainly some aliasing that we cannot quantify. This is why the analysis of the altimetry derived transport focuses on periods larger than 30 days (Z. Koenig et al., manuscript in preparation, 2014), the smoothed transport (with a monthly running mean) variations are robust through all the sensitivity studies. The smoothed transports present reduced standard deviation and reduced ranges (Table 5, Figure 12). However, it should be noted that all the short-term extreme events observed in the altimeter-derived transports, like the minima below 110 Sv in total transport, are not noise: they correspond to specific situations (Z. Koenig et al., manuscript in preparation, 2014).

The method assumes that the vertical structure of the geostrophic velocity field has not changed over the last 20 years. Full-depth velocity structure is scarce at Drake Passage. The only other full depth time series are from Drake 79, 13 years before the beginning of the satellite data and of the reconstructed transport time series. Furthermore, they are located upstream the Shackleton Fracture Zone. The vertical structure of the velocity field was examined in *Ferrari et al*. [2012] and was found similar to the one described in *Inoue* [1985] with a dominance of the of the barotropic and the first baroclinic modes. The data do not indicate changes in the vertical structure of the velocity.

7. Conclusions

The first 20 year long time series of the volume transport (from 1992 to 2012) in the Drake Passage was obtained combining in situ (3 years of current moorings) and satellite altimetric data (20 years). In the course of this research, a new method is needed because of the space and time variability of the narrow fronts in the Drake Passage that make the estimates of cross-track mean velocity profiles from only nine moorings challenging. This method is based on the elaboration of a look-up table of vertical profiles using the current meter data. The look-up table of velocity profiles $B(x, z, v)$ is three-dimensional where x is the position along the track, z the depth, and v the surface velocity. The cross-track mean surface geostrophic velocities were estimated using an error/correction scheme in a sensitivity study to the mean velocities deduced from two recent Mean Dynamic Topographies (MDT): the CNES-CLS09 MDT and the CNES-CLS13 MDT. The internal consistency of the method was assessed with the error/correction scheme.

Comparisons with independent data such as the near bottom current meter velocities from the cDrake experiment near mooring M4 [*Chereskin et al*., 2009], the two consecutive hydrographic transects with LADCP from *Renault et al*. [2011] or the baroclinic transport estimates from the annually repeated hydrographic transect SR1b from 1993 to 2011 [*Cunningham et al*., 2003] proved the method to be reliable. The values of the transport time series at the time of the transects always fell within the error bars of the in situ transport estimates. Comparison with the "classical" method [*Spadone and Provost*, 2009] further demonstrated the consistency and robustness of the method.

Full-depth transports and transports over 3000 m barely differ as the transport below 3000 m is close to zero despite the significant deep velocities. Indeed, in that particular region of Drake Passage, the deep recirculations in the two semiclosed basins (Yaghan and Ona) have a close to zero net transport as westward and eastward flows tend to cancel out in each basin.

Over 20 years, the full-depth volume transport has a mean of 141 Sv (sem 2.7 Sv), a standard deviation of 13 Sv, and a range of 110 Sv. Yearly means vary from 133.6 Sv in 2011 to 150 Sv in 1993 and standard deviations from 8.8 Sv in 2009 to 17.9 Sv in 1995. The canonical ISOS values with a mean of 133.8 Sv and a std of 11.2 Sv obtained from a year-long record in 1979 [*Whitworth*, 1983; *Whitworth and Peterson*, 1985] are very similar to those found here for year 2011 (133.6 Sv and 12 Sv).

The full-depth baroclinic transport over 20 years has a mean of 136 Sv (sem 2.7 Sv), a standard deviation of 11 Sv, and a range of 68 Sv. The average baroclinic transport estimated by *Cunningham et al*. [2003] from the six annually repeated SR1b transects from 1993 to 2000 was 136.7 Sv with a standard deviation of 7.8 Sv (reconstructed: mean 134.4 Sv and std 11.8 Sv). The average baroclinic transport calculated here with the 10 SR1b sections from 2001 to 2011 is 134.4 Sv with a standard deviation of 5.8 Sv (reconstructed: mean 137 Sv and std 10.8 Sv). Yearly means calculated here vary from 144 Sv in 2012 to 122 Sv in 1995 and standard deviation from 8 Sv in 1992 to 13.4 Sv in 1998. The canonical ISOS values correspond to a low mean and an average std in the 20 year long time series.

The full-depth barotropic transport over 20 years has a mean of 5 Sv (sem 4.0 Sv), a standard deviation of 16 Sv, and a range of 119 Sv. The standard deviation of the barotropic transport exceeds that of the baroclinic and total transports. Indeed, barotropic and baroclinic transports are anticorrelated at −0.5 (this anticorrelation is carefully examined in a companion paper).

Measurements were obtained in a very specific spot of the ACC with strong bathymetric constraints. It is most likely that the mean partition between barotropic and baroclinic components vary along the ACC path. It has to be investigated with numerical modeling, this study providing an element of comparison.

In agreement with many authors [*Meredith et al*., 2011; *Böning et al*., 2008], we do not find any significant increase in the volume transport in face of the increasing SAM-index. However, small trends are observed in the different volume transport time series: a small decrease in the total volume transport time series (−3.6 to −8.8 Sv in 20 years), a larger decrease in the barotropic transport time series (−8.8 to −15.5 Sv in 20 years), and a small increase in the baroclinic transport (+4.6 to 9.4 Sv in 20 years). These trends, although barely significant considering the uncertainty on the transport estimates (estimated around 7–10 Sv) are consistently observed regardless of the method (classical or new one) or the surface geostrophic velocity used (adjusted one, or derived from CNES-CLS09/13 MDT).

A detailed spectral analysis of the time series of total volume, baroclinic and barotropic transports, and an examination of the potential dynamical drivers of the observed variations are the object of a companion paper.

Appendix A: Correction of the ADCP Cross-Track Velocitites at M3 in 2006–2008

The gappy cross-track velocities at M3 in 2006–2008 were filled using the statistics derived from the full cross-track velocities gathered at M3 in 2008–2009.

The first EOF of the cross-track velocities $V_2(z, t)$ at M3 in 2008–2009 (ADCP data and deep current meters) explains 97% of the variance, thus $V_2(z, t)$ can be expressed as:

$$V_2(z,t) = V_{2m}(z) + a(t)f(z) \tag{A1}$$

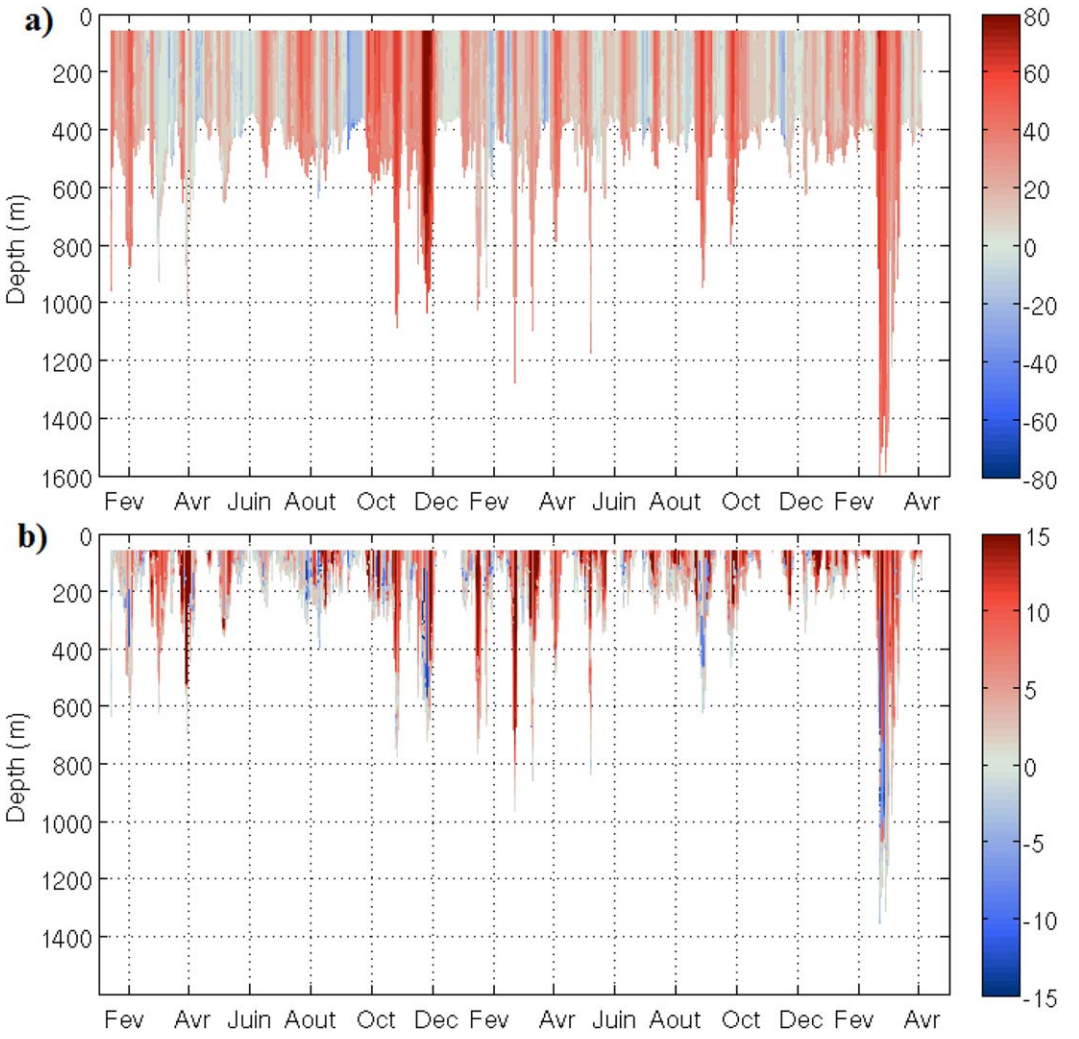

Figure A1. (a) Cross-track ADCP velocities (in cm/s) at M3 in 2006–2008 filled with the method detailed in Appendix A. (b) Difference between the barotropic filled ADCP velocities at M3 in 2006–2008 and the ADCP velocities at M3 in 2006–2008 filled with the method detailed in Appendix A. Velocities (colorbar) are in cm/s. *x* axis is time and *y* axis is depth in meter.

where $V_{2m}(z)$ is the 2008–2009 mean cross-track velocity profile at M3, $f(z)$ the first EOF, and $a(t)$ the associated principal component. The EOFs are calculated after removing the mean vertical profile.

We suppose that the mean shear dV_{2m}/dz and the first EOF $f(z)$ are the same during the two periods, and then during the gappy period, the cross-track velocity $V_1(z, t)$ at $z > z_0$ where z_0 is the uppermost observed level can be written as

$$V_1(z,t) = V_1(z_0,t) + V_{2m}(z) - V_{2m}(z_0) + b(t)(f(z) - f(z_0)) \quad \text{with} \quad z > z_0 \tag{A2}$$

The first term corresponds to a zero shear, the second term to the mean shear correction, and the third to the time-dependent EOF-related term correction. This last correction was small compared to the mean shear correction term. Differences in cross-track velocities filled with the two methods (no shear or the method explained above) are as large as 10 cm/s at the surface for events with an important mooring diving (Figure A1, January 2008).

Appendix B: A Posteriori Comparison With the "Classical" Method

The new method developed to estimate $V(x, z, t)$ is a posteriori compared to the classical method [*Spadone and Provost*, 2009]. The function $A(x, z)$ which characterizes the vertical structure (the correlation between

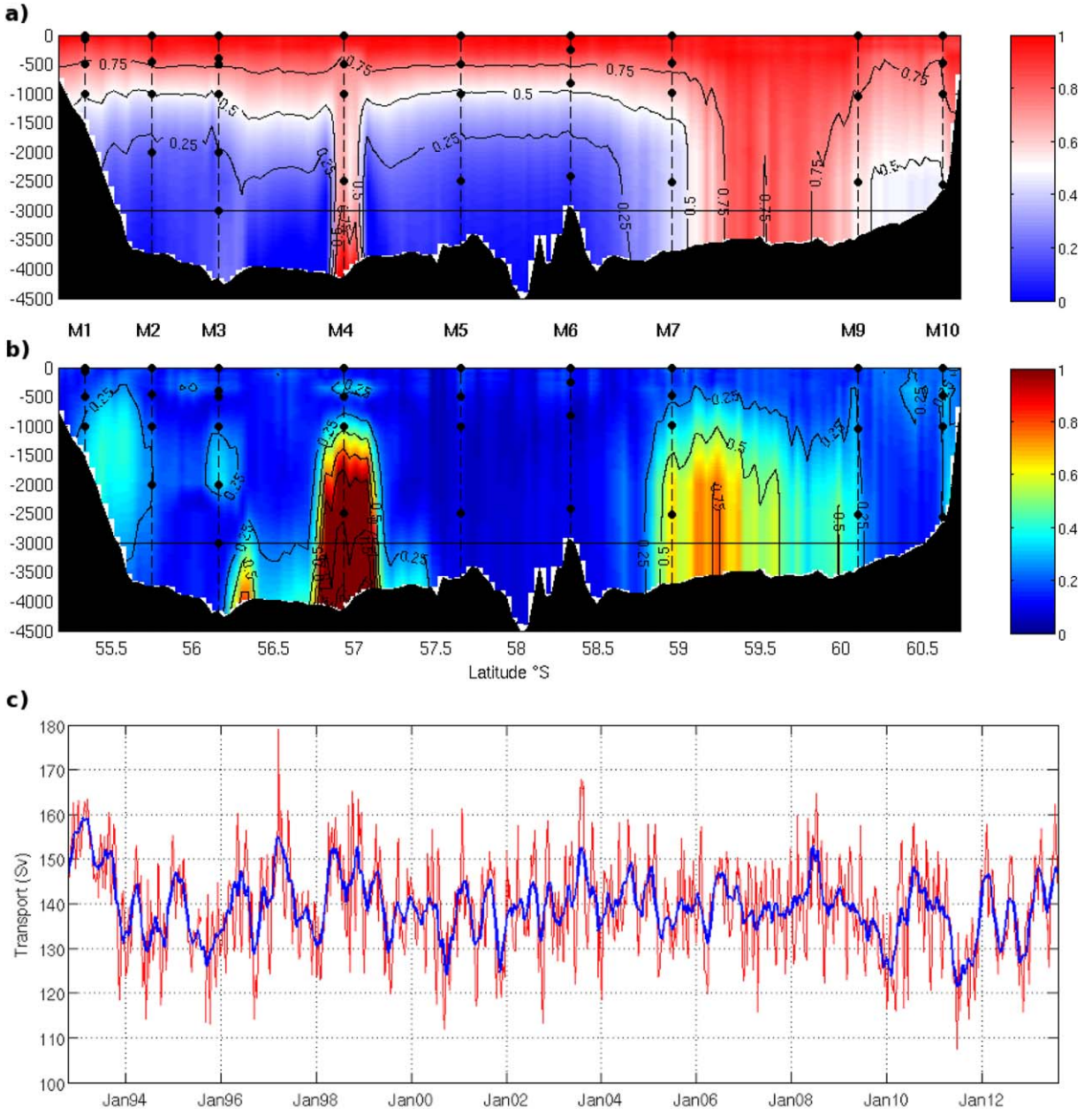

Figure B1. Function A. (a) mean and (b) standard deviation. Bathymetry is shown in solid black. Velocities (colorbar) are in cm/s. *x* axis is latitude (S) and *y* axis is depth in meter. (c) In red, full-depth transport estimated using the "classical" method [*Spadone and Provost*, 2009]. The mean velocities are the one estimated during 2006–2009 (Figure 9a) and the function A is the mean one estimated on the same period (Figure 9c). (Blue) Smoothed transport obtained with a one month running mean. Transport is in Sverdrup.

the velocity at depth z with the surface velocity) in the classical method is independent of time. Here we a posteriori compose a function $A(x, z, t)$ depending on time using relation 1 (section 2.2):

$$A(x,z,t)=\frac{(V(x,z,t)-V_m(x,z))}{V'(x,0,t)} \tag{B1}$$

with $V_m(x, z)$ being the mean cross-track velocities over 2006–2009 deduced from the reconstructed velocities (Figure 11), $V(x, z, t)$ the reconstructed cross-track velocities and $V'(x,0,t)$ the cross-track velocity anomalies computed from the SLA.

The structure of the mean function A (averaged over time) $A_m(x, z)$ (Figure B1a) shows a barotropic structure in the center of the Ona Basin and a baroclinic one in the Yaghan Basin. The area around 60°S (the location of the SACCF-S), is less barotropic than the rest of the Ona Basin. The function A at M4 presents a large barotropic component, caused by the deep recirculation cell as expected from Figure 6 (M4 plot).

The standard deviation of A shows spatial disparities. Note that, by construction, at the surface A is always 1 and the standard deviation of A is zero. Although smaller than 0.2 in general, the std of A can reach values in excess of 1 (Figure B1b). The largest std values of A are found around the deep recirculation cell at M4 (values up to 2), consistent with a reasonable correlation (0.48) with the deep c-Drake current meter observations. In the Ona Basin, std values of A are large (above 0.5) over a large part of the water column between 59° and 59.5°S which is likely related to large std values of A observed at depth (Figure 14b).

The distributions of the mean value of A and of the std of A make sense. This a posteriori check showed that the new method developed to estimate cross-track velocities provided coherent results when put in the framework of the former method.

For the purpose of comparison, we recalculated the volume transport using the classical method:

$$V(x,z,t) = V_m(x,z) + A(x,z)V'(x,z,t) \tag{B2}$$

with the mean A and the mean velocities $V_m(x, z)$ estimated a posteriori from the new method (Figure B1c). The mean total volume transport from the surface to the bottom is 139 Sv, 2 Sv smaller than that from the new method. The std is smaller (11,4 Sv instead of 13 Sv for 7 day resolution, 6.6 Sv instead of 7.6 Sv for the smoothed transport) for the classical method. The smoothed transport trend from the "classical method" and the "new method" (Figure 12b) are very close. The root mean square (rms) of the difference between the volume transport time series from the two methods is 7.5 Sv, and the rms of the difference between the smoothed transports is 3.6 Sv. The same general linear trends are observed: a small decrease in the total volume transport time series, a stronger decrease in the barotropic transport time series, and a small increase in the baroclinic transport.

Acknowledgments

This paper is a contribution to the DRAKE project that was funded both by CNES (Centre National d'Etudes Spatiales) through the OST/ST altimetric program and by CNRS-INSU (Institut des Sciences de l'Univers) through the LEFE program. We gratefully acknowledge Eberhard Fahrbach and AWI staff for their support for sea-going operations and the captains and crews of the RV Polarstern. We thank Annie Kartavtseff for the ADCP data processing and Pr. Young-Hyang Park for most valuable comments on the manuscript. The current meter data and the LADCP hydrographic sections are available at LOCEAN, the SR1B hydrographic transects at NOC, and the altimetry data at AVISO (CLS Argos). The SR1b hydrographic transects used in this work were funded by the UK Natural Environment Research Council through research programmes at the National Oceanography Centre and the British Antarctic Survey.

References

Barré, N., C. Provost, A. Renault, and N. Sennéchael (2011), Mesoscale activity in Drake Passage during the cruise survey ANT-XXIII/3: A satellite perspective, *Deep Sea Res., Part II*, *58*(25), 2533–2554, doi:10.1016/j.dsr2.2011.01.003.

Böning, C. W., A. Dispert, M. Visbeck, S. Rintoul, and F. U. Schwarzkopf (2008), The response of the antarctic circumpolar current to recent climate change, *Nat. Geosci.*, *1*(12), 864–869.

Brink, K. (1991), Coastal-trapped waves and wind-driven currents over the continental shelf, *Annu. Rev. Fluid Mech.*, *23*, 389–412, doi: 10.1146/annurev.fl.23.010191.002133.

Bruinsma, S., C. Forste, O. Abrikosov, J.-C. Marty, M.-H. Rio, S. Mulet, and S. Bonvalot (2013), The new ESA satellite-only gravity field model via the direct approach, *Geophy. Res. Lett.*, *40*, 3607–3612, doi:10.1002/grl.50176.

Bryden, H. (1979), Poleward heat flux and conversion of available potential energy in Drake Passage, *J. Mar. Res.*, *37*, 1–22.

Chereskin, T., K. Donohue, D. Watts, K. Tracey, Y. Firing, and A. Cutting (2009), Strong bottom currents and cyclogenesis in Drake Passage, *Geophy. Res. Lett.*, *36*, L23602, doi:10.1029/2009GL040940.

Chouaib, N., F. Stoehr, and C. Provost (2006), Variability of the subantarctic and polar fronts in the Drake Passage as deduced from altimetry, *J. Mar. Res.*, *64*(5), 669–693.

Cunningham, S., S. Alderson, B. King, and M. Brandon (2003), Transport and variability of the Antarctic Circumpolar Current in Drake Passage, *J. Geophy. Res.*, *108*(C5), 8084, doi:10.1029/2001JC001147.

Ferrari, R., C. Provost, A. Renault, N. Sennéchael, N. Barré, Y.-H. Park, and J. Lee (2012), Circulation in Drake Passage revisited using new current time series and satellite altimetry: 1. The Yaghan Basin, *J. Geophy. Res.*, *117*, C12024, doi:10.1029/2012JC008264.

Ferrari, R., Provost, N. Sennéchael, and J. Lee (2013), Circulation in Drake Passage revisited using new current time series and satellite altimetry: 2. The Ona Basin, *J. Geophy. Res.*, *118*, 147–165, doi:10.1002/2012JC008193.

Firing, Y., T. Chereskin, and M. Mazloff (2011), Vertical structure and transport of the antarctic circumpolar current in Drake passage from direct velocity observations, *J. Geophys. Res.*, *116*, C08015, doi:10.1029/2011JC006999.

Firing, Y., T. Chereskin, D. Watts, K. Tracey, and C. Provost (2014), Computation of geostrophic streamfunctions, its derivatives and error estimates from an array of CPIES in Drake Passage, *J. Atmos. Oceanic. Technol.*, *31*, 656–680, doi:10.1175/jtech-d-13-00142.1.

Fyfe, J., and O. Saenko (2007), Simulated changes in the extratropical Southern Hemisphere winds and currents, *Geophys. Res. Lett.*, *33*, L06701, doi:10.1029/2000JC000277.

García, M., I. Bladé, V. Z. Cruzado, A., H. García, J. Puigdefábregas, and J. Sospreda (2002), Observed variability of water properties and transport on the World Ocean Circulation Experiment SR1b section across the antarctic circumpolar current, *J. Geophy. Res.*, *107*(C10), 3162, doi:10.1029/2000JC000277.

Griesel, A., M. Mazloff, and S. Gille (2012), Mean dynamic topography in the southern ocean: Evaluating antarctic circumpolar current transport, *J. Geophys. Res.*, *117*, C01020, doi:10.1029/2011JC007573.

Hall, A., and M. Visbeck (2002), Synchronous variability in the Southern Hemisphere atmosphere, sea ice, and ocean resulting from the Annular Mode, *J. Clim.*, *15*, 3043–3057.

Hallberg, R., and A. Gnanadesikan (2006), The role of eddies in determining the structure and response of the wind-driven Southern Hemisphere overturning: results from the Modeling Eddies in the Southern Ocean (MESO) project, *J. Phys. Oceanogr.*, *36*, 2232–2252.

Inoue (1985), Modal decomposition of the low-frequency currents and baroclinic instability at Drake Passage, *J. Phys. Oceanogr.*, *15*, 1157–1181.

Koshlyakov, M., I. Lisina, E. Morozov, and R. Tarakanov (2007), Absolute geostrophic currents in the Drake Passage based on observations in 2003 and 2005, *Oceanology*, *47*(4), 451–463.
Lenn, Y.-D., T. K. Chereskin, J. Sprintall, and E. Firing (2007), Mean jets, mesoscale variability and eddy momentum fluxes in the surface layer of the antarctic circumpolar current in Drake passage, *J. Mar. Res.*, *65*(1), 27–58, doi:10.1357/002224007780388694.
Meredith, M., and A. M. Hogg (2006), Circumpolar response of southern ocean eddy activity to a change in the southern annular mode, *Geophy. Res. Lett.*, *33*, L16608, doi:10.1029/2006GL026499.
Meredith, M. P., et al. (2011), Sustained monitoring of the southern ocean at drake passage: past achievements and future priorities, *Rev. Geophys.*, *49*, RG4005, doi:10.1029/2010RG000348.
Morrison, A. K., and A. Hogg (2013), On the relationship between southern ocean overturning and acc transport, *J. Phys. Oceanogr.*, *43*(1), 140–148.
Munday, D. R., H. L. Johnson, and D. P. Marshall (2013), Eddy saturation of equilibrated circumpolar currents, *J. Phys. Oceanogr.*, *43*(3), 507–532.
Nowlin, J. W., T. Whitworth, and R. Pillsbury (1977), Structure and transport of the Antarctic circumpolar current at Drake passage from short-term measurements, *J. Phys. Oceanogr.*, *7*, 778–802.
Orsi, A. H., I. T. Whitworth, and J. W. Nowlin (1995), On the meridional extent and fronts of the antarctic circumpolar current, *Deep Sea Res., Part I*, *42*, 641–673.
Provost, C., A. Renault, N. Barré, N. Sennéchael, V. Garçon, J. Sudre, and O. Huhn (2011), Two repeat crossings of Drake passage in austral summer 2006: Short-term variations and evidence for considerable ventilation of intermediate and deep waters, *Deep Sea Res., Part II*, *58*(25–26), 2555–2571, doi:10.1016/j.dsr2.2011.06.009.
Renault, A., C. Provost, N. Sennéchael, N. Barré, and A. Kartavsteff (2011), Two full-depth velocity sections in the Drake Passage in 2006: Transport estimates, *Deep Sea Res., Part II*, *58*(25), 2572–2591, doi:10.1016/j.dsr2.2011.06.009.
Rio, M., S. Guihenut, and G. Larnicol (2011), New CNES-CLS09 global mean dynamic topography computed from the combination of GRACE data, altimetry and in situ measurements, *J. Geopys. Res.*, *116*, C07018, doi:10.1029/2010JC006505.
Rio, M.-H., S. Mulet, and N. Picot (2013), New global Mean Dynamic Topography from a GOCE geoid model, altimeter measurements and oceanographic in situ data, ESA Living Planet Symposium, Edinburg.
Schaeffer, P., P. Faugére, J. Legeais, A. Ollivier, T. Guinle, and N. Picot (2012), The CNES-CLS11 Global Mean Sea Surface computed from 16 years of satellite altimeter data, *Mar. Geod.*, *35*(sup1), 3–19.
Spadone, A., and C. Provost (2009), Variations in the Malvinas Current volume transport since October 1992, *J. Geophys. Res.*, *114*, C02002, doi:10.1029/2008JC004882.
Sprintall, J. (2003), Seasonal to interannual upper-ocean variability in the Drake Passage, *J. Mar. Res.*, *61*(1), 27–57, doi:10.1357/002224003321586408.
Thompson, D. J. W., and S. Solomon (2002), Interpretation of recent southern hemisphere climate change, *Science*, *296*(5569), 895–899.
Toggweiler, J., and B. Samuels (1995), Effect of Drake passage on the global thermohaline circulation, *Deep Sea Res., Part I*, *42*(4), 477–500.
Vivier, F., and C. Provost (1999), Direct velocity measurements in the malvinas current, *J. Geophys. Res.*, *104*(C9), 21,083–21,103, doi:10.1029/1999JC900163.
Whitworth, T. (1983), Monitoring the transport of the antarctic circumpolar current at Drake passage, *J. Phys. Oceanogr.*, *13*, 2045–2057.
Whitworth, T., and R. Peterson (1985), Volume transport of the Antarctic Circumpolar Current from bottom pressure measurements, *J. Phys. Oceanogr.*, *15*, 810–816.
Whitworth, T., W. Nowlin, and S. Worley (1982), The net transport of the antarctic circumpolar current through Drake passage, *J. Phys. Oceanogr.*, *31*, 960–971.
Wunsch, C. (1998), The work done by the wind on the oceanic general circulation, *J. Phys. Oceanogr.*, *28*(11), 2332–2340.
Yang, X.-Y., D. Wang, J. Wang, and R. Huang (2007), Connection between the decadal variability in the Southern Ocean circulation and the Southern Annular Mode, *Geophys. Res. Lett.*, *34*, L16604, doi:10.1029/2007GL030526.